LITHOS 514-515 (2025) 108185

Contents lists available at ScienceDirect

LITHOS

journal homepage: www.elsevier.com/locate/lithos

Variable onset of magma segregation controls contrasting geochemical patterns of mineral assemblages in fractionating alkaline volcanic systems

Thomas Binder [a,*], Michael A.W. Marks [a], Tobias Fusswinkel [b], Benjamin F. Walter [a], Gregor Markl [a]

[a] Department of Geosciences, Eberhard Karls Universität Tübingen, Schnarrenbergstraße 94–96, 72076 Tübingen, Germany
[b] Institute of Applied Mineralogy and Economic Geology, Rheinisch-Westfälische Technische Hochschule Aachen, Wüllnerstraße 2, 52056 Aachen, Germany

ARTICLE INFO

Keywords:
Agpaitic mineral assemblage
Alkaline rocks
Central European Volcanic Province
Clinopyroxene
Ijolite
Perovskite

ABSTRACT

Three occurrences of primitive, alkaline, SiO_2-undersaturated, volcanic rocks from SW Germany show coarse-grained, mm- to cm-thin veinlets and pockets of differentiated lithologies that are a missing link in an evolutionary trend towards phonolites. (1) In the Hegau region (Hohenstoffeln), melilite-bearing olivine nephelinite contains ijolite pockets with skeletal perovskite, titanomagnetite, and euhedral fluorapatite. (2) Compositionally similar olivine melilitite at Urach (Sternberg) is crosscut by ijolite veinlets with late-magmatic lileyite and wadeite, in which subhedral–euhedral titanomagnetite and perovskite lack a skeletal shape. (3) Nepheline syenitic domains in a phlogopite-nepheline basanite from the Kraichgau region (Steinsberg) contain less clinopyroxene, titanomagnetite, and apatite, but accessory titanite. Differences between the fractionation products partly result from variable host magma compositions. However, the exact starting point of residual melt separation was the key factor explaining the trace element evolution of late mineral phases. Under conditions of advanced clinopyroxene crystallization and perovskite saturation (Urach), massive trace element fractionation led to high Nb/Ta and Zr/Nb, but low LREE/HREE and Zr/Hf ratios in clinopyroxene and perovskite. High F contents contributed to the stabilization of LILE, Zr, and Hf in the enriched residual melt which finally caused crystallization of an agpaitic assemblage. In contrast, melt separation before perovskite saturation (Hegau) resulted in strong, uniform enrichment of LILE, HFSE, and REE in clinopyroxene and perovskite. The nepheline syenite (Kraichgau) underwent a similar evolution with incompatible element enrichment in clinopyroxene and titanite, although its mineral assemblage differs from the ijolites due to higher SiO_2 and H_2O but lower F and P concentrations in the melt.

1. Introduction

Alkaline volcanic rocks occur frequently in the context of intraplate magmatism (e.g., Circum-Mediterranean anorogenic Cenozoic igneous province; Serra Do Mar igneous province, Brazil; High Arctic Large Igneous Province, Canada; Alaotra, Ankaratra and Takarindiona districts, Madagascar; Bédard et al., 2021; Chmyz et al., 2025; Lustrino and Wilson, 2007; Mazzeo et al., 2021; Melluso et al., 2011). They are often found in continental rift systems (e.g., Baikal Rift Zone, East African Rift System, Rio Grande Rift, Gardar province, Oslo Graben, European Cenozoic Rift System), but also on ocean islands (e.g., Canary Islands, Hawaii, Kerguelen, Tristan da Cunha) and in ring-dyke complexes without clear tectonic control (e.g., Alnö, Sweden; Kola, Russia; Tchivira, Angola; Cameroon Line; Magnet Cove, Arkansas; Binder et al., 2023; Braunger et al., 2018; Dawson, 2008; Flohr and Ross, 1990; Gill, 2010; Schmitt et al., 2024; Vuorinen et al., 2005).

In few cases, the entire sequence from primitive olivine melilitites, olivine nephelinites, and/or basanitic nephelinites via intermediate rocks (e.g., basanites, tephrites, phonotephrites, tephriphonolites) to evolved phonolites is exposed in single volcanoes or districts (e.g., Kaiserstuhl, Germany; Labe tectono-volcanic zone, Czech Republic; Tenerife, Canary Islands; Essimingor, Tanzania; Braunger et al., 2018; Mana et al., 2012; Sliwinski et al., 2015; Vaněčková et al., 1993). In many cases, however, individual volcanic edifices or entire alkaline provinces are characterized by bimodal volcanism. This feature is associated with the lack of intermediate rocks, a phenomenon known as

* Corresponding author.
E-mail addresses: thomas.binder@uni-tuebingen.de (T. Binder), michael.marks@uni-tuebingen.de (M.A.W. Marks), tobias.fusswinkel@emr.rwth-aachen.de (T. Fusswinkel), benjamin.walter@uni-tuebingen.de (B.F. Walter), gregor.markl@uni-tuebingen.de (G. Markl).

https://doi.org/10.1016/j.lithos.2025.108185
Received 16 April 2025; Received in revised form 3 July 2025; Accepted 5 July 2025
Available online 10 July 2025
0024-4937/© 2025 The Authors. Published by Elsevier B.V. This is an open access article under the CC BY license (http://creativecommons.org/licenses/by/4.0/).

Daly Gap (e.g., Oldoinyo Lengai, Tanzania; Saghro, Morocco; Hegau, Heldburg and Lusatia, Germany; Abratis et al., 2015; Berger et al., 2009; Binder et al., 2024b; Büchner et al., 2015; Keller et al., 2006; Klaudius and Keller, 2006). As the magmatic sequence is thus not exposed completely, differentiation trajectories and fractionation mechanisms for Ca- and Mg-rich, SiO_2-undersaturated, alkaline melts are elusive at the emplacement level. However, cumulate fragments (wehrlites, pyroxenites, foidolites, foid syenites) entrained in primitive volcanic rocks indicate the existence of evolving and continuously fed magma chambers (Berger et al., 2009; Binder et al., 2024b; Mourey et al., 2023; Platz et al., 2004; Ulrych et al., 2005).

Rare mesocratic to leucocratic, coarse-grained veinlets and pockets of foidolitic to foid syenitic compositions in such primitive volcanic products are interpreted as in-situ and low-pressure differentiates that crystallize during and/or shortly after emplacement of their hosts (e.g., Binder et al., 2024b; Ulrych et al., 2000). The limited volumes of segregated melt, coupled with rapid cooling, lead to the "freezing" of these assemblages, inhibiting the typical fractionation processes that would otherwise progress to phonolitic compositions. Therefore, they are promising candidates to fill the *Daly gap* as the missing link in bimodal alkaline magmatic provinces and to improve understanding of the causative processes underlying magma separation and differentiation.

This contribution focuses on textural observations and mineral chemistry data for three occurrences of primitive volcanic host rocks in the Central European Volcanic Province (CEVP) that contain rare, evolved, coarse-grained domains (ijolites, nepheline syenite). Unlike plutonic xenoliths and autoliths in Eger Graben, Eifel, Hegau, and Kaiserstuhl (Binder et al., 2024b; Braunger et al., 2018; Schmincke, 2007; Ulrych et al., 2000, 2005), such structures are products of *syn*-eruptive melt separations and allow deciphering the mechanisms behind differentiation processes that occur during the crystallization of melilititic, nephelinitic, and basanitic rocks. The results show that, despite numerous similarities among the occurrences, distinct evolution trends are realized depending on the initial melt composition and the onset of containment of the residual melts, especially regarding volatiles and incompatible elements. These are expressed in the occurrence of various accessory minerals and trace element patterns of clinopyroxene, perovskite, and titanite.

2. Geological setting

The CEVP is part of the circum-Mediterranean anorogenic Cenozoic igneous province (Lustrino and Wilson, 2007) and comprises diverse volcanic regions and individual volcanic structures in central and southern Germany, the Czech Republic, western Poland, and eastern France (Binder et al., 2023). The southern part of the CEVP (Fig. 1a) is dominated by primitive sodic melilititic, nephelinitic, and basanitic rocks, with the polygenetic Kaiserstuhl and rare evolved (phonolitic) haüynites, haüyne nephelinites, and phonolites from the Hegau and Odenwald representing prominent exceptions (Binder et al., 2023, 2024b; Braunger et al., 2018; Mann et al., 2006). The area comprises

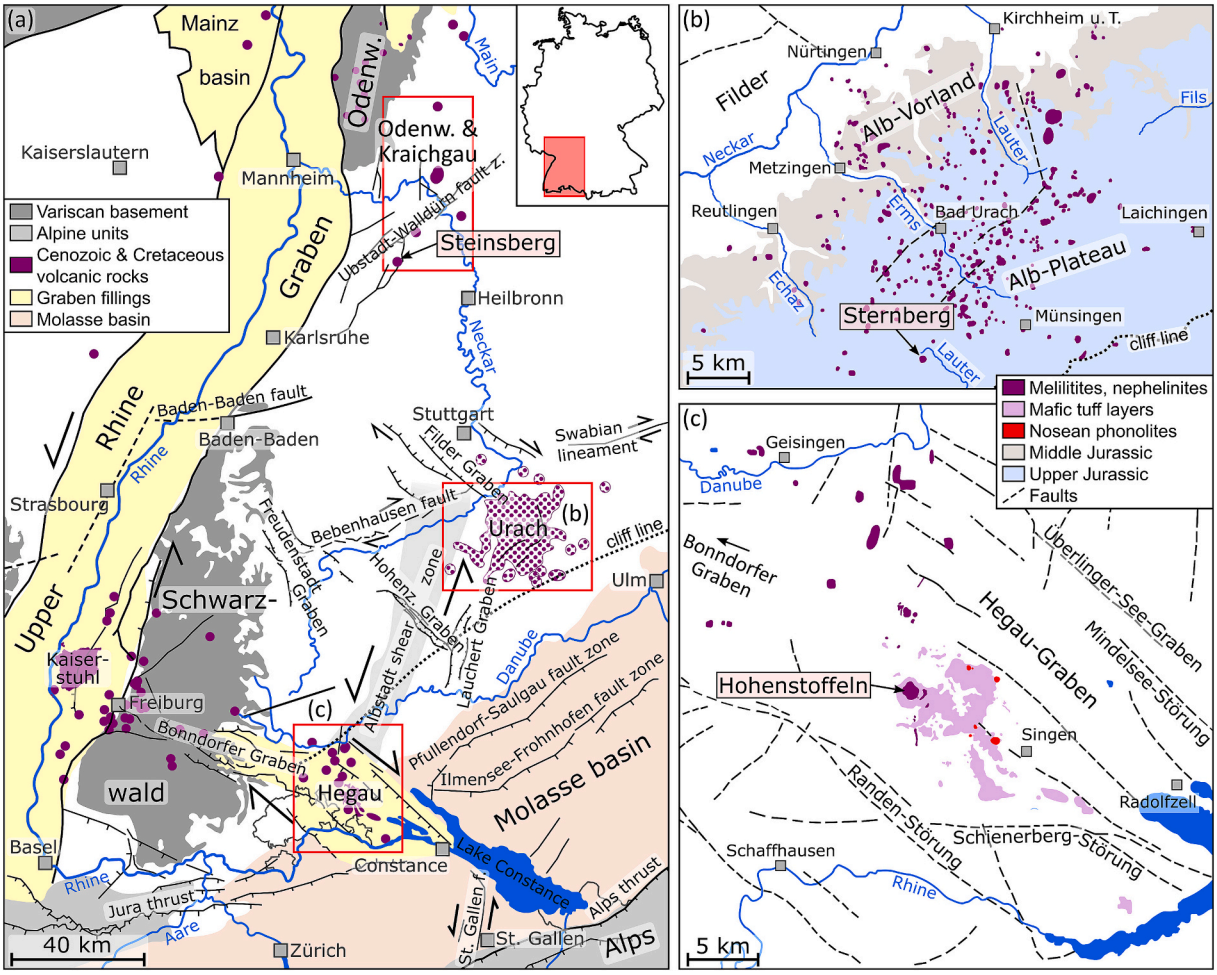

Fig. 1. Simplified geologic maps showing (a) the southern CEVP with major tectonic structures and the studied regions outlined (modified after Egli et al., 2017 and Binder et al., 2024a), (b) the Urach volcanic field, and (c) the Hegau region. The three localities with evolved domains are Steinsberg (nepheline syenite; Kraichgau region), Sternberg (ijolite; Urach volcanic field) and Hohenstoffeln (ijolite; Hegau region).

two distinct age groups of volcanic rocks:

- Upper Cretaceous to Eocene (~73–47 Ma) melilite-free olivine nephelinites, basanitic nephelinites, and nepheline basanites in the Taunus, the Lower Main plain, the Odenwald and Kraichgau, the Vosges and Pfälzerwald, and the Bonndorfer Graben and Freiburger Bucht region, plus haüyne nephelinites, haüynites, and phonolitic haüynites restricted to the Odenwald,
- Oligocene to Miocene (~27–9 Ma) perovskite-bearing olivine melilitites and melilite-bearing olivine nephelinites in the Hegau region, at Urach, in the southern Upper Rhine Graben, and in Lorraine, with nosean phonolites occurring only in the Hegau region (Binder et al., 2023).

The two rock series derive from two different mantle sources. The older ones formed by up to 6 % partial melting of amphibole-bearing garnet(−spinel) lherzolite at the base of the lithosphere in a source metasomatized by hydrous melts or fluids (Binder et al., 2024a). The younger group was produced by low-degree partial melting of an amphibole ±phlogopite-bearing garnet wehrlite in the uppermost asthenosphere, which underwent CO_2- and Ca-rich subduction-related metasomatism (Alibert et al., 1983; Binder et al., 2024a; Blusztajn and Hegner, 2002; Dunworth and Wilson, 1998; Hegner and Vennemann, 1997).

The present study focuses on three specific localities in three distinct volcanic regions, namely the Odenwald and Kraichgau area (Steinsberg; Horn et al., 1972), the Urach volcanic field (Sternberg; Hegner et al., 1995), and the Hegau region (Hohenstoffeln; Blusztajn and Hegner, 2002; Fig. 1). The volcanic outcrops in the Kraichgau area are linked to the Ubstadt-Walldürn fault zone, while the Urach area is located at the north-eastern tip of the N-S directed seismically active Albstadt shear zone adjacent to several smaller faults, including the Filder, Lauchert, and Hohenzollern grabens and the Swabian lineament (Mader et al., 2021; Rupf and Nitsch, 2008). The Hegau region lies at the southern end of the Albstadt shear zone, merging into the NW-SE trending Hegau Graben, the eastern extension of the WNW-ESE oriented Bonndorfer Graben. At all three localities, coarse-grained domains occur as several mm- to cm-thin veinlets or pockets within the fine-grained to porphyritic primitive volcanic rocks, features that have not yet been found anywhere else in the southern CEVP.

Steinsberg is the southernmost of eight volcanic structures in the Odenwald and Kraichgau area (Fig. 1a) and has an age of 55.2 Ma (+3.9/−3.3 Ma) determined using the K—Ar method (Horn et al., 1972). Recent in-situ U—Pb apatite and zircon ages from five other localities in the same region yield older ages of ~62–70 Ma (Binder et al., 2023; Schmitt et al., 2007). The volcanic body has partly the composition of a (phonolitic) phlogopite-nepheline basanite and partly of a basanitic phlogopite nephelinite and hosts nepheline syenitic veinlets.

Sternberg is an olivine melilitite occurrence in the southernmost part of the Urach volcanic field, which consists of over 350 geomagnetically proven vents that are only partially exposed (Fig. 1b; Mäussnest, 1974). Coarse-grained pockets and irregularly distributed veinlets are of ijolitic composition and found in a small, abandoned quarry a few decametres west of the Sternberg summit. Their age was determined to be 12.65 ± 0.45 Ma using the in-situ U—Pb method on perovskite and matches that of the host rock (13.95 ± 2.32 Ma), consistent with a *syn*- to late-magmatic origin (Binder et al., 2023).

Hohenstoffeln is located in the central part of the Hegau region, which comprises ~25 isolated vents/necks and, more rarely, dykes of melilite-bearing olivine nephelinites and nepheline-bearing olivine melilitites in the northwest and centre, and six nosean phonolite domes in the east (Fig. 1c; Mäussnest and Schreiner, 1982), associated with smaller mafic tuff vents and extensive tuff blankets. Rare ijolitic pockets and veinlets at Hohenstoffeln volcano are found in the abandoned quarry at the summit. Apatite and perovskite from two ijolite samples yielded in-situ U—Pb ages of 11.1–9.7 Ma (Binder et al., 2023).

3. Material and methods

For petrographic examination and rock classification according to Le Maitre et al. (2002), 19 thin sections from seven localities of the three regions (Table 1; Hegau, Urach, Odenwald and Kraichgau) were studied by polarization and scanning electron microscopy. The samples originate from collections of the University of Tübingen and the State Office for Geology, Raw Materials and Mining in Freiburg (Germany); in addition, the localities Hohenstoffeln, Steinsberg, and Sternberg were resampled to augment the inventory. One sample from each of the seven localities (comprising ijolite, nepheline syenite, nephelinite, melilitite, haüynite, nepheline basanite) was selected for LA-ICP-MS analyses. Electron probe microanalyses (EPMA) were performed on the two ijolite

Table 1
Sample list including locality name, coordinates, and rock type.

Sample	Locality	Latitude (°N)	Longitude (°E)	Rock type
HEG 02	Hohenstoffeln	47.794465	8.750537	Ijolite
HEG 03	Hohenstoffeln	47.794465	8.750537	Mll-b. olivine nephelinite, ijolite
HEG 03a	Hohenstoffeln	47.794465	8.750537	Mll-b. olivine nephelinite
HEG 04	Hohenstoffeln	47.794465	8.750537	Nepheline olivine melilitite
HEG 05	Hohenstoffeln (EPMA, LA-ICP-MS)	47.794465	8.750537	Ijolite
HEG 17	Hohenhewen (LA-ICP-MS)	47.835623	8.747227	Mll-b. olivine nephelinite, ijolite
M 10	Donnstetten (LA-ICP-MS)	48.514918	9.566112	Nepheline-b. olivine melilitite
U 001	Sternberg (EPMA, LA-ICP-MS)	48.394731	9.379102	Ijolite
U 016	Sternberg	48.394731	9.379102	Olivine melilitite
U 018	Dietenbühl (LA-ICP-MS)	48.453687	9.484991	Phl-b. melilite olivine nephelinite
I 20	Waldbrunn (LA-ICP-MS)	49.484208	9.040353	Phonolitic ol-b. nph haüynite
N 17	Steinsberg near Weiler	49.296643	8.952210	Phonolitic phl nepheline basanite
N 19	Steinsberg near Weiler	49.296643	8.952210	Phonolitic phl nepheline basanite, Phl-b. nepheline syenite
N 265	Steinsberg near Weiler	49.296643	8.952210	Basanitic phlogopite nephelinite
Stb I	Steinsberg near Weiler	49.214967	8.877751	Basanitic phlogopite nephelinite
Stb II	Steinsberg near Weiler	49.214543	8.877808	Phlogopite-nepheline basanite
Stb III	Steinsberg near Weiler (EPMA, LA-ICP-MS)	49.214123	8.877179	Phlogopite-nepheline basanite, Phl-b. nepheline syenite
Stb IV	Steinsberg near Weiler	49.214059	8.877382	Phlogopite-nepheline basanite
Stb V	Steinsberg near Weiler	49.213781	8.877526	Phlogopite-nepheline basanite, Phl-b. nepheline syenite

b. – bearing; EPMA – electron probe microanalyses performed on the sample for this study; LA-ICP-MS – LA-ICP-MS analyses performed on the sample for this study; mll – melilite; nph – nepheline; ol – olivine; phl – phlogopite.

samples (Hohenstoffeln, Sternberg) and a single nepheline syenite sample (Steinsberg; Table 1) from the three localities. The mineral compositions were compared with those of the primitive volcanic rocks of the same regions (Binder et al., 2024a, 2024b). For details on the application of clinopyroxene-based geothermobarometry according to Neave and Putirka (2017), Putirka (2008), and Wang et al. (2021), see Supplementary material, File 1.

3.1. EPMA

Mineral compositions (major and minor elements) were analysed using a *JEOL JXA 8230* electron probe microanalyzer in wave-length dispersive mode at the Department of Geosciences, University of Tübingen. The specific sensitivities of the mineral surfaces to the probe current depend on the chemical composition and were a critical factor in adjusting the configurations. Peak count times were fixed at 10 s for light and volatile elements (Na, F), 16 s for the other major elements and 30 s for minor elements, with background count time set to half of the respective peak count time. Calibration was carried out by synthetic and natural standards, and peak overlap corrections (Cr—V, V—Ti, F—Fe, F—Ce, Ce—Ba, Pr—La, Ba—Ti). An internal φ(ρz) raw data correction was performed for all analyses except the oxyspinel analyses, for which ZAF correction was applied. Specific parameters for the analytical protocols and all results are given in the *Mendeley Data* repository (see *Data availability*).

Mineral formula and endmember calculations were performed according to Deer et al. (2009). The Fe^{3+}/Fe^{2+} determination in clinopyroxene, titanomagnetite, ilmenite/hematite, pseudobrookite, lileyite, and wadeite was carried out assuming an ideal lattice site occupancy of 4, 3, 2, 3, 12, and 6 cations per formula unit, respectively. Apatite formulas were calculated based on $\Sigma\ OH + F + Cl = 1$ and $\Sigma\ PO_4^{3-} + SO_4^{2-} + SiO_4^{4-} = 3$ anions.

3.2. LA-ICP-MS

Trace element compositions in individual crystals of clinopyroxene, perovskite, titanite, apatite, and lileyite in the thin sections were analysed using a *Coherent GeolasHD* 193 nm laser ablation system coupled with an *Agilent 7900 s* quadrupole ICP-MS with high sensitivity s-lens configuration and operated with Pt skimmer and sampler cones (Institute of Applied Mineralogy and Economic Geology, RWTH Aachen University). Instrumental accuracy was monitored by daily five-fold replicate measurements of NIST612 across the entire mass range using NIST610 as the external reference material and reference values from the GeoREM certified values database (Jochum et al., 2007, 2011). Instrument tuning was carried out daily for optimization of sensitivities, stable ablation, transport, and ionization conditions (U/Th = 1.00 ± 0.02) as well as minimalization of oxide formation (ThO/Th <0.3 %) and doubly charged interference production rates (Ca^{2+}/Ca <0.3 %). For mineral ablation, laser fluence was set to 4 J/cm^3 and 5 or 10 Hz repetition rate at beam diameters of 24–60 μm, depending on mineral, crystal size, and thickness of the thin sections. The background signal was measured for 40 s, and the ablation time was >40 s if possible.

Sample measurements were bracketed by NIST 610 and BCR 2G as external reference materials and quality control standards. Quantification of the results (^{7}Li, ^{11}B, ^{23}Na, ^{24}Mg, ^{27}Al, ^{29}Si, ^{39}K, ^{44}Ca, ^{45}Sc, ^{47}Ti, ^{55}Mn, ^{56}Fe, ^{59}Co, ^{60}Ni, ^{63}Cu, ^{66}Zn, ^{71}Ga, ^{72}Ge, ^{85}Rb, ^{88}Sr, ^{89}Y, ^{90}Zr, ^{93}Nb, ^{133}Cs, ^{137}Ba, ^{139}La, ^{140}Ce, ^{141}Pr, ^{146}Nd, ^{147}Sm, ^{153}Eu, ^{157}Gd, ^{159}Tb, ^{163}Dy, ^{165}Ho, ^{166}Er, ^{169}Tm, ^{172}Yb, ^{175}Lu, ^{178}Hf, ^{181}Ta, ^{182}W, ^{208}Pb, ^{232}Th, ^{238}U in silicates and perovskite, plus ^{31}P, ^{34}S, ^{75}As in apatite) was performed with the *PySILLS* data reduction software (Beeskow et al., 2022; Guillong et al., 2008), using the reference material NIST 610 as external standard. The CaO content of clinopyroxene, perovskite, titanite, and apatite and the SiO_2 content of lileyite, each known from microprobe analyses, served as internal standard for determination of the absolute element concentrations. An integration interval of ~30 s was selected for the background, as well as for the analysed mineral, if possible. The Grubbs test with a threshold value of 2000 was used to detect and eliminate spikes for data smoothing. All results, lower limits of detection and uncertainties (1σ) are given in the *Mendeley Data* repository (see *Data availability*). The systematic use of acronyms for groups of incompatible elements in the following sections is shown in Table 2.

3.3. Rayleigh fractional crystallization modelling

Average Sr and Sc contents of clinopyroxene phenocrysts from the host rocks of the ijolites were used to model the evolution of clinopyroxene composition with respect to these two elements, assuming Rayleigh fractional crystallization and using published partition coefficients for clinopyroxene and melilite in equilibrium with a melilititic melt (Minissale et al., 2019). For simplification, it was assumed that precipitation of olivine is largely complete at the beginning of clinopyroxene crystallization. This is supported by the microstructure of the two host rocks, as olivine occurs exclusively in the form of macrocrysts, while clinopyroxene accounts for major amounts of the groundmass and its macrocrysts are less abundant and smaller than those of olivine (Fig. 2b, d). Only clinopyroxene and melilite in different ratios were assumed fractionating phases, which is justifiable as cogenetic minerals (e.g., nepheline, oxides) are negligible in quantity and/or very incompatible for both Sc and Sr.

In the Rayleigh equation used (1), C_i is the concentration of trace element i in the melt, C_0 is the initial concentration in the melt, F_L the remaining melt fraction, and $\overline{D_i}$ the weighted average partition coefficient for the respective element:

$$C_i = C_0 F_L^{\overline{D_i}-1} \quad (1)$$

C_i was calculated from the measured average trace element concentration in cores of clinopyroxene phenocrysts in the host rock and from the partition coefficient D_i^{Cpx} for melilititic melts. $\overline{D_i}$ was calculated as shown in Eq. 2, with X_m being the mass fraction of a fractionating mineral m in relation to the total mass of all fractionating phases with the partition coefficient D_i^m for the element i:

$$\overline{D_i} = \sum_m X_m \bullet D_i^m = X_{Cpx} \bullet D_i^{Cpx} + X_{Mll} \bullet D_i^{Mll} \quad (2)$$

The expected trace element concentration in clinopyroxene (C_i^{Cpx}), in equilibrium with a given fraction of residual melt and a specified clinopyroxene-to-melilite ratio, was calculated using Eq. 3, D_i^{Cpx} denoting the partition coefficient of the element between clinopyroxene and melt:

$$C_i^{Cpx} = C_0 F_L^{\overline{D_i}-1} \bullet D_i^{Cpx} \quad (3)$$

The values used for the parameters of the equations for the modelling are listed in Table 3.

Table 2
Groups of incompatible elements and their acronyms.

Acronym	Group of incompatible elements	Elements
HFSE	high-field-strength elements	Zr, Hf, Nb, Ta, Th, U
LILE	large-ion lithophile elements	K, Rb, Cs, Sr, Ba
REE	rare-earth elements	La, Ce, Pr, Nd, Sm, Eu, Gd, Tb, Dy, Ho, Er, Tm, Yb, Lu
LREE	light rare-earth elements	La, Ce, Pr, Nd
MREE	middle rare-earth elements	Sm, Eu, Gd, Tb, Dy
HREE	heavy rare-earth elements	Ho, Er, Tm, Yb, Lu

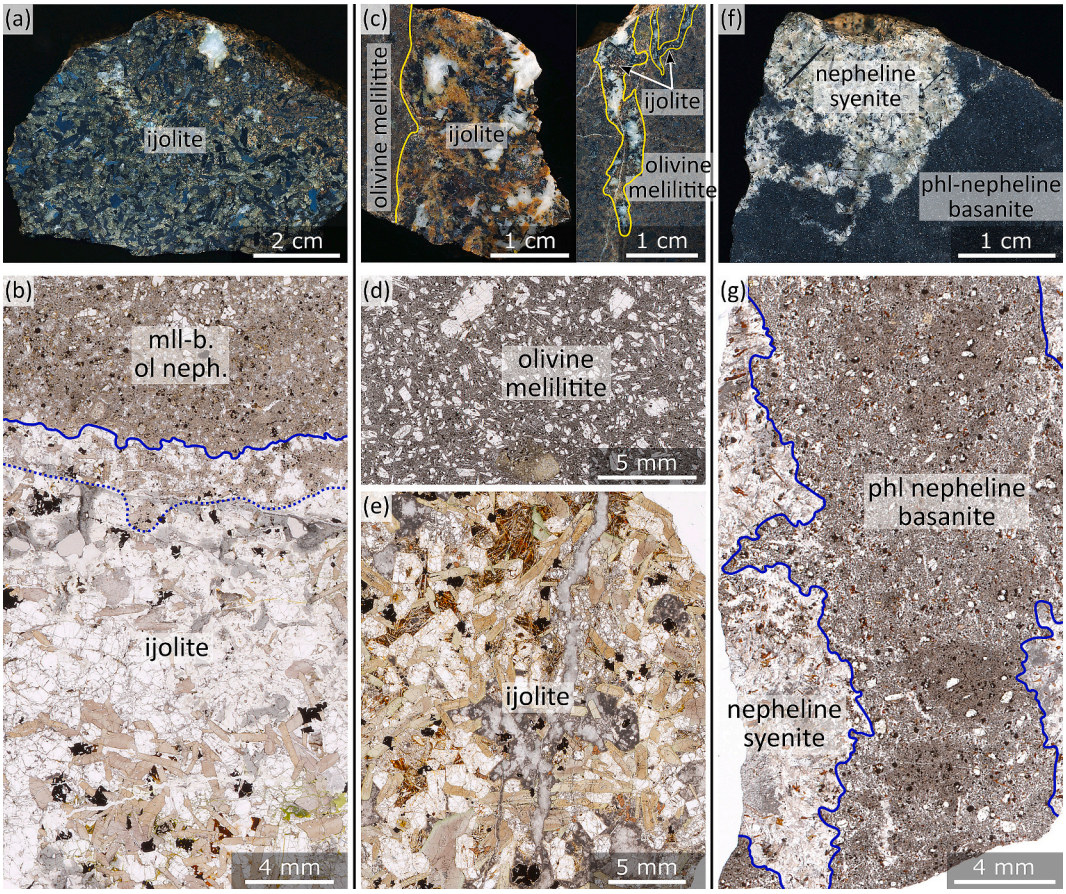

Fig. 2. Petrographic features of plutonic domains in the volcanic rocks of the southern CEVP. (a) Ijolite within (b) a melilite-bearing olivine nephelinite from the Hohenstoffeln volcano (Hegau), showing euhedral tabular nepheline, sector- and concentrically zoned subhedral–euhedral clinopyroxene, and skeletal magnetite. (c) Ijolitic pockets and veinlets found within (d) an olivine melilitite from the Sternberg volcano (Urach), exhibiting (e) euhedral tabular nepheline, sector- and concentrically zoned subhedral–euhedral clinopyroxene, euhedral magnetite, and perovskite. (f) Nepheline syenite within a phlogopite-nepheline basanite from the Steinsberg (Kraichgau), showing (g) subhedral–euhedral tabular phlogopite, alkali feldspar, altered nepheline, clinopyroxene, and euhedral magnetite.

4. Results

4.1. Petrography

Based on mineralogical composition and microstructure, primitive melilititic to foiditic and basanitic rocks as well as evolved ijolitic and nepheline syenitic domains were distinguished.

4.1.1. Hegau

The primitive porphyritic volcanic rocks represent melilite-bearing olivine nephelinites and nepheline-bearing olivine melilitites with olivine (20–40 vol%), clinopyroxene (5–20 vol%), melilite (<10 vol%), and occasionally euhedral medium-grained haüyne macrocrysts (<5 vol %), embedded in a groundmass of euhedral clinopyroxene (10–35 vol %), titanomagnetite (10–15 vol%), melilite (<20 vol%), subhedral–anhedral nepheline (<20 vol%), interstitial phlogopite/kinoshitalite (<5 vol%), and accessory euhedral perovskite and apatite. Olivine crystals comprise variable proportions of euhedral–subhedral phenocrysts and subhedral–anhedral, rounded, partly sheared, fractured xeno- and antecrysts. Euhedral yellowish–reddish brown clinopyroxene macrocrysts often show concentric and/or hourglass sector zoning.

At the Hohenstoffeln locality, melilite-bearing olivine nephelinite encloses coarse-grained ijolitic domains (Fig. 2a) bounded by a few millimetres wide transition zone, bridging the compositional and textural differences to the volcanic host (Fig. 2b). The ijolite contains subhedral–euhedral tabular nepheline (50–60 vol%, including alteration and replacement products like zeolites and carbonates), complex sector-zoned and concentrically zoned brownish to reddish clinopyroxene (~30 vol%), frequently with green rims (Fig. 3a-c), and skeletal titanomagnetite (~10 vol%; Fig. 3b). This assemblage is flanked by early magmatic euhedral elongated apatite needles (<5 vol%), and purple skeletal crystals and crystal clusters of perovskite (Fig. 3c).

4.1.2. Urach

The primitive volcanic rocks are mostly porphyritic nepheline-bearing olivine melilitites similar to those from the Hegau region (Fig. 2c, d). However, their melilite content (max. 40 vol%) is higher on average at the expense of clinopyroxene (<30 vol%) and nepheline (<10 vol%). Melilite phenocrysts may reach the size of olivine macrocrysts (20–50 vol%) and accessory kalsilite microcrysts are present.

At the Sternberg locality, ijolitic veins and veinlets that crosscut olivine melilitite (Fig. 2c) are composed of subhedral–euhedral tabular nepheline (45–55 vol%, including alteration and replacement products), complex sector-zoned and concentrically zoned reddish-brown to greenish clinopyroxene (~35 vol%), euhedral titanomagnetite (<10 vol %), and subhedral orange to brownish perovskite (~5 vol%; Fig. 3d-f). Euhedral elongated apatite needles (<5 vol%) are common, often enclosed by clinopyroxene, titanomagnetite, and nepheline (Fig. 3d-f). Lath-shaped, orange to yellowish lileyite crystals are present as interstitial minerals (Figs. 3f and 4), usually accompanied by small subhedral wadeite and euhedral Sr-rich apatite (Fig. 4). The mineral assemblage is partially altered to zeolites, carbonates, mica, Fe hydroxides, and clay minerals (Figs. 2e, 3d, e and 4).

Table 3
Parameters and values used for Rayleigh fractional crystallization modelling.

Parameter	Explanation	Values
i	trace element	Sc, Sr
C_o	expected concentration of the trace element in the initial melt based on the measured average clinopyroxene core composition in the volcanic host rocks and D_i^{Cpx} for melilititic melts	Hohenstoffeln: 40.5 μg/g Sc, 501 μg/g Sr Sternberg: 53.4 μg/g Sc, 412 μg/g Sr
F_L	remaining melt fraction	1.0; 0.9; 0.8; 0.7; 0.6; 0.5; 0.4; 0.3; 0.2; 0.1; 0.05; 0.03; 0.01
m	mineral	clinopyroxene, melilite
X_{Cpx}	mass fraction of fractionating clinopyroxene	0.0; 0.25; 0.50; 0.75; 0.90; 1.0
X_{Mll}	mass fraction of fractionating melilite	0.0; 0.10; 0.25; 0.50; 0.75; 1.0
D_{Sc}^{Cpx}	partition coefficient for Sc between clinopyroxene and melilititic melt	4.03 (avg. from Minissale et al., 2019)
D_{Sc}^{Mll}	partition coefficient for Sc between melilite and melilititic melt	0.31 (avg. from Minissale et al., 2019)
D_{Sr}^{Cpx}	partition coefficient for Sr between clinopyroxene and melilititic melt	0.38 (avg. from Minissale et al., 2019)
D_{Sr}^{Mll}	partition coefficient for Sr between melilite and melilititic melt	1.82 (avg. from Minissale et al., 2019)
C_i	concentration of a trace element in the melt	value to be calculated
C_i^{Cpx}	trace element concentrations to be expected in clinopyroxene at given mass fractions of residual melt and given clinopyroxene-to-melilite ratios	value to be calculated

4.1.3. Odenwald and Kraichgau

Two volcanic rock groups occur in this region, one of which represents (phonolitic) phlogopite-nepheline basanites or basanitic phlogopite nephelinites. These are composed of olivine (15–30 vol%), subhedral lath-shaped phlogopite (max. 25 vol%), and few euhedral yellowish brownish sector-zoned and concentrically zoned clinopyroxene phenocrysts (~5 vol%), embedded in a groundmass of nepheline (~10 vol%), clinopyroxene (10–30 vol%), titanomagnetite (10–20 vol%), plagioclase (<15 vol%), alkali feldspar (<5 vol%), and accessory apatite. The second group comprises evolved (phonolitic) haüynites and haüyne nephelinites with euhedral haüyne–nosean–sodalite$_{ss}$ (10–20 vol%), apatite (<10 vol%), subhedral–euhedral olivine (<10 vol%), titanomagnetite (15–20 vol%; often with ilmenite exsolution lamellae), and subhedral poikilitic beige to yellowish clinopyroxene macrocrysts (15–25 vol%) enclosing euhedral titanomagnetite and apatite. The groundmass consists of beige to greenish clinopyroxene needles, anhedral titanomagnetite, nepheline (<10 vol%), sanidine (<10 vol%), apatite, and interstitial amphibole and phlogopite (<5 vol%).

At the Steinsberg locality, nepheline syenitic domains are hosted by a phlogopite-nepheline basanite (Fig. 2f, g) and characterized by subhedral lath-shaped alkali feldspar (30 vol%), tabular nepheline (20–30 vol%, including alteration products), subhedral–euhedral phlogopite (~15 vol%), euhedral brownish to reddish clinopyroxene (5–10 vol%), and subhedral titanomagnetite (5–10 vol%; Fig. 3g-i). Accessories are small apatite needles, subhedral–euhedral titanite (Fig. 3h, i), and rare pseudobrookite.

4.2. Mineral chemistry

4.2.1. Clinopyroxene

Clinopyroxene in the volcanic rocks is mostly dominated by diopside and hedenbergite components (>60 mol%; Fig. 5a) with the Tschermak components reaching up to 40 mol%. The Na pyroxene endmembers (mostly <5 mol% aegirine, Ti aegirine, jadeite) are elevated in the nephelinitic to basanitic rocks of the Odenwald and Kraichgau area (max. 18 mol%, predominantly aegirine). Haüyne-rich rocks of the same region contain aegirine-dominated crystals in the groundmass. Clinopyroxene crystals in the coarse-grained domains of all three localities largely resemble the composition of those in the volcanic rocks. They exhibit normal, reverse, or oscillatory concentric zoning that depends on slight differences in the onset and duration of crystallization as well as on cogenetic minerals and their respective compositional evolution. This feature is often superimposed by sector zoning. Nevertheless, aegirine (max. 21 mol%) and hedenbergite components generally increase towards the outer rims of all crystals in the coarse-grained rocks, with the latter varying between localities (Fig. 5b; Hegau max. 50 mol% hedenbergite, Urach 22 mol%, Kraichgau 15 mol%). Contents of Al and Ti reach up to 0.6 and 0.22 apfu, respectively, at a broadly constant X_{Mg} of ~0.8–1.0, with only small differences between plutonic domains and volcanic rocks (Fig. 5c, d). However, more evolved rims in the ijolites show a separate trend with low Al (0.02–0.05 apfu) and Ti contents (0.04–0.07 apfu) at lower X_{Mg} (Hegau ~0.35–0.65, Urach ~0.75–0.80). This can also be observed in the evolved haüyne-rich volcanic rocks in the Odenwald and Kraichgau, although Ti (0.05–0.21 apfu) is subject to scatter.

The Zr content reaches up to ~3400 μg/g in the Urach ijolite but only ~1500 μg/g in the Hegau ijolite and Kraichgau nepheline syenite (Fig. 5e). Some crystals in the evolved volcanic rocks of the Odenwald and Kraichgau region show exceptionally high Zr concentrations (max. 1.3 wt%). The evolution of trace element concentrations in clinopyroxene is very different between the regions and localities (Figs. 6 and 7). In the Kraichgau nepheline syenite and Urach ijolite, Sr concentrations are ~140–430 μg/g with increased values in crystal rims of the latter (<1070 μg/g), while clinopyroxene from the Hegau ijolite shows higher Sr concentrations both in cores (~260–630 μg/g) and rims (max. 2350 μg/g; Fig. 6a). The same is true for the evolved volcanic rocks from the Odenwald and Kraichgau (~800–2000 μg/g), whereas clinopyroxene in the primitive volcanic rocks from all regions has low Sr concentrations (~100–470 μg/g). The contents of Ge (2–4 μg/g) and V (~110–480 μg/g) in clinopyroxene from the volcanic rocks overlap and increase with increasing Zr in the plutonic domains, albeit with distinct trajectories, the highest concentrations occurring in the Urach ijolite (up to 9 μg/g Ge and 1250 μg/g V; Fig. 6b, c).

Scandium in clinopyroxene is strongly enriched in the Urach ijolite (max. 850 μg/g) compared to the surrounding volcanic rocks (20–260 μg/g), while the Hegau ijolite, the Kraichgau nepheline syenite, and the evolved volcanic rocks from Odenwald and Kraichgau area show a depletion for Sc in clinopyroxene (9–110 μg/g) relative to the primitive volcanic rocks (110–155 μg/g; Fig. 6d). In contrast, Y contents in clinopyroxene of the Urach ijolite (5–22 μg/g) resemble those in the melilitites, nephelinites, and basanites (8–41 μg/g; Fig. 6e). In clinopyroxene of the Hegau ijolite (21–39 μg/g), the Kraichgau nepheline syenite (15–102 μg/g), and the haüyne-rich Odenwald and Kraichgau rocks (51–87 μg/g), however, Y shows significantly higher average values and correlates positively with the Zr contents. Thorium concentrations in clinopyroxene are low in all primitive volcanic rocks (<0.8 μg/g) and increase with increasing Zr in the Hegau ijolite (0.4–1.8 μg/g) and in the Kraichgau nepheline syenite (0.1–0.9 μg/g) but decrease below the detection limit in the Urach ijolite (<10 ng/g; Fig. 6f).

Chondrite-normalized REE patterns for clinopyroxene macrocrysts from all volcanic rocks show an enrichment of LREE over HREE (Fig. 7a). The Hegau ijolite and the Kraichgau nepheline syenite have increased REE contents in clinopyroxene compared to their host rocks. In contrast, clinopyroxene in the Urach ijolite is strongly depleted in LREE and MREE, showing partly subchondritic values, whereas only the three heaviest REE show higher concentrations than in the host rock clinopyroxene. Both the primitive volcanic rocks from Urach and Hegau regions contain late clinopyroxene microcrysts, the patterns of which deviate from the general trend and exhibit LREE and MREE depletion, a slightly positive Eu anomaly, and HREE enrichment.

The contents of Hf and Nb correlate positively with the Zr content (Fig. 7b, c). While Hf contents in clinopyroxene of the volcanic rocks

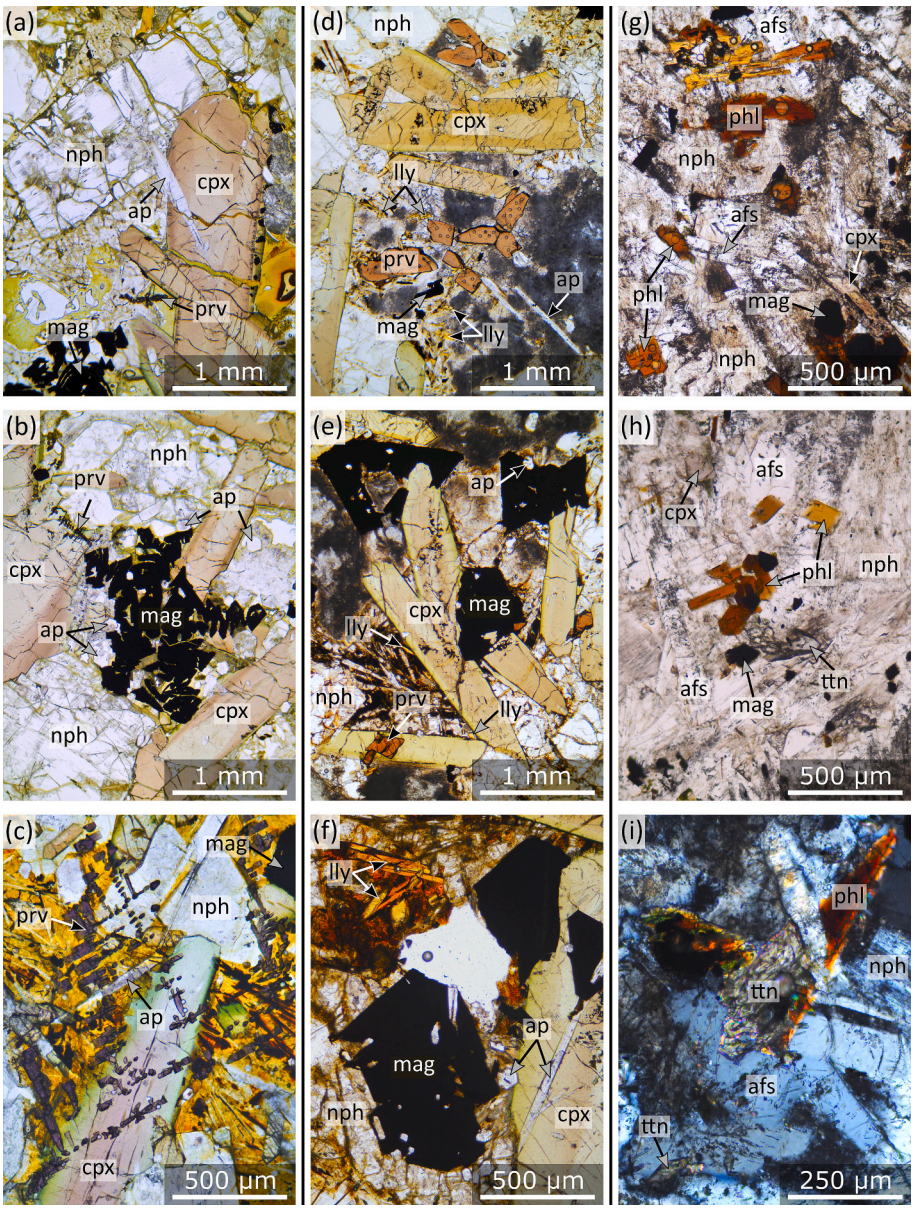

Fig. 3. Microphotographs of the evolved plutonic domains of the southern CEVP. (a) Ijolite from the Hohenstoffeln volcano (Hegau), showing euhedral tabular nepheline (nph), sector- and concentrically zoned subhedral–euhedral clinopyroxene (cpx), needles and hexagonal cross-sections of apatite (ap), skeletal euhedral–subhedral (b) magnetite (mag) and (c) purple perovskite (prv) crystals. (d) Ijolite from the Sternberg volcano (Urach), exhibiting euhedral tabular nepheline, sector- and concentrically zoned subhedral–euhedral clinopyroxene, subhedral crystals and crystal groups of brown–orange perovskite, and (e) skeletal euhedral magnetite, accompanied by (f) needles and hexagonal cross-sections of apatite, and euhedral–subhedral lath-shaped lileyite (lly) crystals. (g) Nepheline syenite from the Steinsberg volcano (Kraichgau), showing subhedral–euhedral tabular phlogopite (phl), alkali feldspar (afs), altered nepheline, clinopyroxene, and euhedral magnetite with (h + i) accessory subhedral–euhedral titanite (ttn) crystals. (For interpretation of the references to colour in this figure legend, the reader is referred to the web version of this article.)

resemble those in the coarse-grained domains (2–40 µg/g), except for the Urach ijolite (up to 130 µg/g Hf), Nb contents are lower in the primitive volcanic rocks and the Urach ijolite (0.3–12 µg/g) and higher in the Hegau ijolite (3–38 µg/g), in the nepheline syenite (0.8–17 µg/g), and in the evolved volcanic rocks of the Odenwald and Kraichgau region (4–74 µg/g). The Zr/Hf ratios in clinopyroxene in the Urach ijolite (24–34) are lower than in the Hegau ijolite (36–87). The Kraichgau nepheline syenite has intermediate ratios (24–39) and all host rocks show similarly low values (18–47; Fig. 7d). In contrast, the Nb/Ta ratios in clinopyroxene are far higher in the Urach ijolite (33–288) than in the Hegau ijolite (4–28) and in the Kraichgau nepheline syenite (5–6), while all host rocks show ratios of ~4–10 (rarely up to 27; Fig. 7e).

4.2.2. *Fe—Ti oxides*

Most opaque phases in the plutonic domains are magnetite–ulvöspinel$_{ss}$ with 46–74 mol% ulvöspinel component in the ijolites and 20–63 mol% in the nepheline syenite. The volcanic rocks contain Fe—Ti oxides with similar compositions (Fig. 8a), but also comprise Mg-

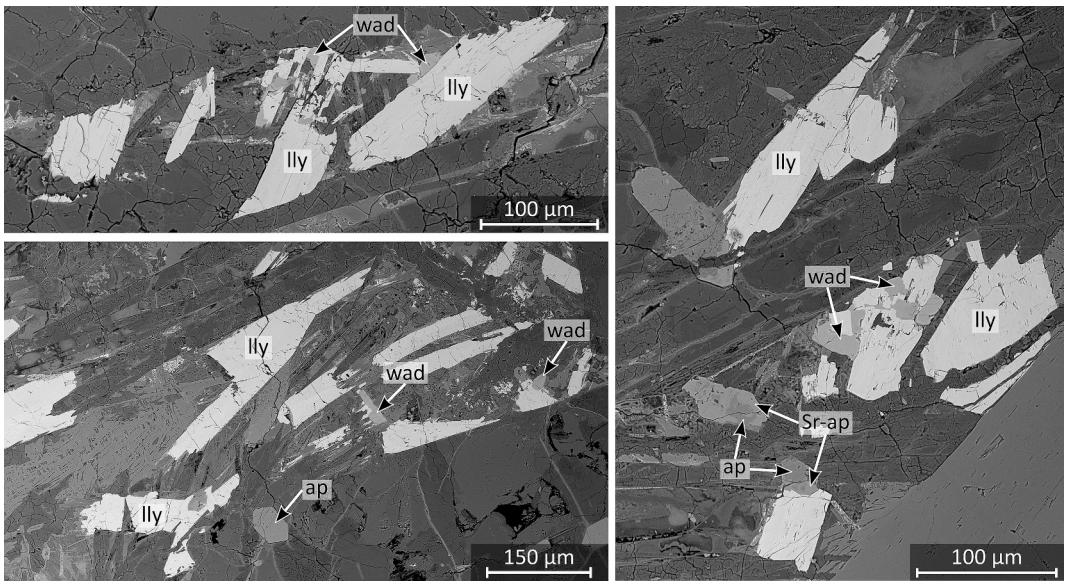

Fig. 4. Late-stage assemblage of euhedral–subhedral lileyite (lly) with smaller amounts of subhedral wadeite (wad) crystals accompanied by apatite and Sr-rich apatite in interstices of the Sternberg ijolite (Urach).

Al-Cr spinel endmembers with low Fe^{3+}+Ti contents (0.12–1.80 apfu; Fig. 8b-d). The higher Fe content in titanomagnetite of the Kraichgau nepheline syenite is explained by exsolution of ilmenite lamellae. More oxidized Fe—Ti oxides adjacent to a line between ilmenite and hematite/maghemite (Fig. 8a) are alteration and weathering products. Pseudobrookite is restricted to Odenwald and Kraichgau samples and was also reported in a haüyne phonolite and a syenite dyke from the Katzenbuckel volcano in the same region (Stähle and Koch, 2003).

Manganese contents in oxyspinel (<0.07 apfu) increase with increasing Fe^{3+}+Ti contents. Few crystals in the volcanic rocks and the nepheline syenite from the Odenwald and Kraichgau region have markedly higher values (max. 0.21 apfu; Fig. 8b). The Zn concentration in oxyspinel from these rocks is also significantly higher (550–13,000 µg/g) than in the Urach and Hegau ijolites (140–830 µg/g), whose values resemble those of the volcanic rocks from the same regions (<2600 µg/g; Fig. 8c). In contrast, the V contents are low in oxyspinel of the Kraichgau nepheline syenite (1200–2500 µg/g) but significantly elevated at high Fe^{3+}+Ti contents in the ijolites (Hegau 2300–5900 µg/g, Urach 5300–10,000 µg/g) compared to most of the volcanic rocks (Fig. 8d).

4.2.3. Perovskite and titanite

Perovskite in the two ijolites and their host rocks displays remarkably different evolution trajectories (Figs. 9 and 10). Skeletal perovskite in the Hegau ijolite is more enriched in several incompatible elements (e.g., Na, Sr, Nb, Ta, LREE) than perovskite in the primitive volcanic rocks, although the initial point of the mineral chemical evolution in the ijolite is in the compositional range of host rock perovskite. In contrast, the concentrations of many incompatible elements in subhedral perovskite in the Urach ijolite are lower than those in the primitive host rocks (e.g., Na, Nb, Ta, LREE, Th, Fig. 9b, c, e). The Fe content in perovskite of both ijolites decreases relative to that in perovskite of the volcanic rocks (Fig. 9f). Uranium and Ba concentrations in perovskite correlate positively with Nb and are similarly enriched in the ijolites as in the host rocks of the respective region, with perovskite in the Urach rocks showing lower Nb_2O_5 (0.6–1.1 wt%), U (26–240 µg/g), and Ba concentrations (7–74 µg/g) than in the Hegau rocks (3.2–7.2 wt% Nb_2O_5, 334–834 µg/g U, 77–260 µg/g Ba; Fig. 10b, c).

Zirconium, Hf, and W in perovskite correlate positively and deviate from the trends of other incompatible elements. They are enriched in the Urach ijolite (566–709 µg/g Zr) but depleted in the Hegau ijolite (171–238 µg/g Zr), compared to the associated volcanic rocks (197–430 µg/g and 400–748 µg/g Zr, respectively; Fig. 10d-f). The Zr/Hf and Nb/Ta ratios of perovskite in the Hegau ijolite resemble those in the volcanic rocks (50–70 and 16–53, respectively), while Zr/Hf ratios are slightly lower (25–40) and Nb/Ta ratios significantly higher (25–105) in perovskite in the Urach ijolite than in the volcanic rocks (28–58 and 7–29, respectively; Fig. 10g). Chondrite-normalized REE patterns for perovskite show a strong enrichment of LREE over HREE in all rocks, although this enrichment is much less pronounced in the Urach ijolite, as a conspicuous trough has developed from Ce to Dy (Fig. 10h).

Titanite occurs exclusively in the Kraichgau nepheline syenite; the crystals are strongly but irregularly zoned, frequently reaching a very high Zr content (max. 0.14 apfu; Fig. 11a). Positive correlations exist between Nb (max. 0.07 apfu) and Na (max. 0.03 apfu) and between LREE+Y (max. 0.03 apfu) and Al + Fe^{3+} contents (0.06–0.13 apfu; Fig. 11b, c). The chondrite-normalized REE pattern shows a strong enrichment of LREE over MREE and HREE and a slightly negative Eu anomaly (Eu/Eu* = 0.34–0.71; Fig. 11d).

4.2.4. Apatite

In the ijolite from Urach, fluorapatite has almost endmember compositions (max. 3 mol% chlorapatite component), while in the primitive host rocks, it contains up to 12 mol% chlorapatite and 25 mol% hydroxyapatite fractions (Fig. 12a). The same range is covered by the volcanic rocks of the Hegau region, but apatite in the associated ijolite evolves towards lower F contents with up to 30 mol% hydroxyapatite and 13 mol% chlorapatite. Primitive volcanic rocks in the Odenwald and Kraichgau area contain hydroxyapatite ($OH_{46–76}F_{20–47}Cl_{3–9}$ ap) or fluorapatite ($F_{46–88}OH_{11–42}Cl_{10–19}$ ap), evolving to F-rich and Cl-poor compositions ($F_{70–88}OH_{10–24}Cl_{1–7}$ ap) in the Kraichgau nepheline syenite.

The sulphate contents are highest in the more evolved haüyne-rich volcanic rocks (~0.06–0.10 apfu) and likewise elevated in the primitive rocks from the Odenwald and Kraichgau area (max. ~0.05 apfu; Fig. 12b). In contrast, the sulphate contents in apatite in the melilititic–nephelinitic rocks, in the ijolites, and in the nepheline syenite are low (<0.025 apfu). Vanadium concentrations in apatite are below the detection limit in the Odenwald and Kraichgau rocks but elevated in some of the Hegau rocks and highest in the Urach rocks (max. ~0.02 apfu), each including the ijolite (Fig. 12c).

There are no significant differences between apatite in the different

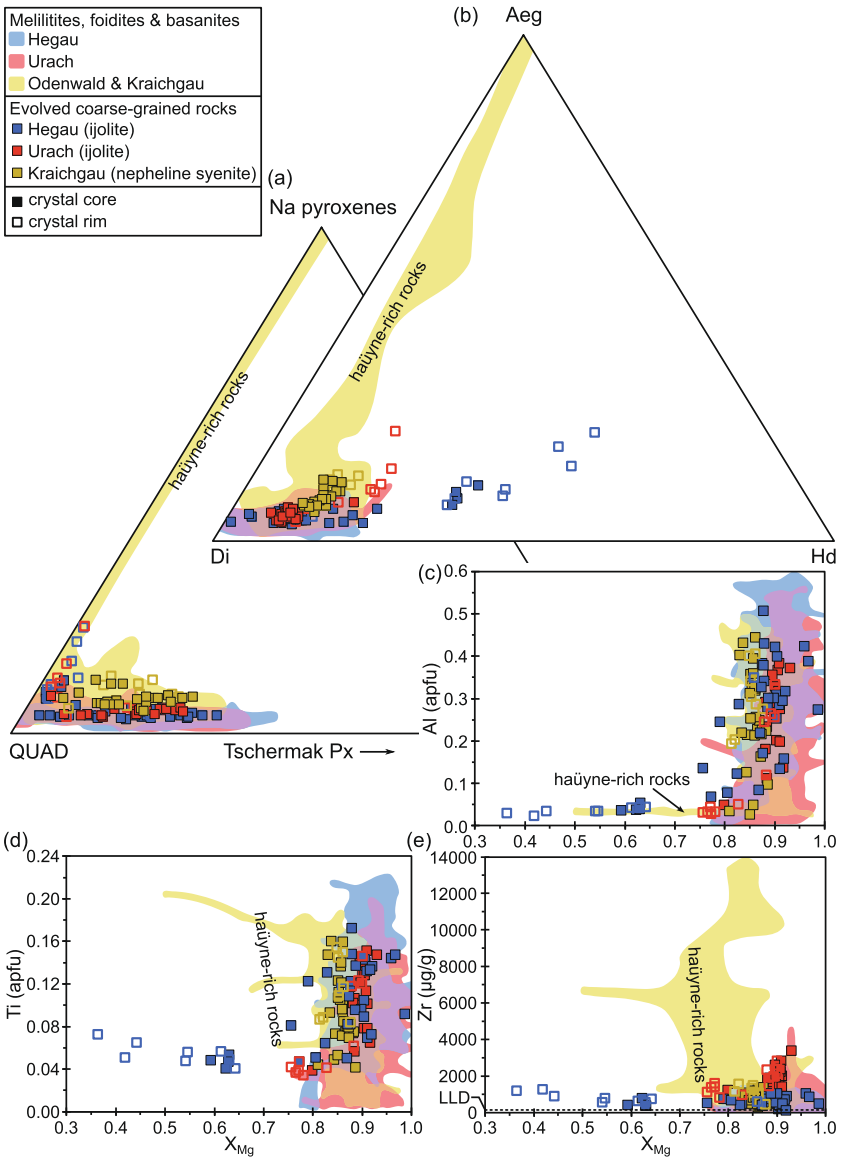

Fig. 5. Clinopyroxene composition in the investigated igneous rocks. EPMA data of this work is supplemented by Binder et al. (2024a, 2024b) and Mann et al. (2006). Solid squares represent crystal cores and empty squares crystal rims. (a) Triangular plot showing the distribution among the quadrilateral endmembers (QUAD), Tschermak clinopyroxenes ($CaXXSiO_6$ with X = Al, Fe^{3+}, Cr, Ti), and Na pyroxenes (aegirine – $NaFe^{3+}Si_2O_6$, Ti aegirine – $NaFe^{2+}_{0.5}Ti_{0.5}Si_2O_6$, jadeite – $NaAlSi_2O_6$). (b) Triangular plot showing the distribution among the endmembers diopside (Di), aegirine (Aeg), and hedenbergite (Hd) normalized to 100 %. X_{Mg} = $Mg/(Mg + Fe^{2+})_{molar}$ vs. (c) Al, (d) Ti, and (e) Zr. apfu – atoms per formula unit; LLD – lower limit of detection.

rock types regarding Na, Sr, and REE, except for apatite in the Urach ijolite, which is remarkably low in REE but occasionally enriched in Sr (max. 5 mol% Sr apatite component; Supplementary material, Fig. A1). The chondrite-normalized REE pattern shows a continuous decrease of REE enrichment from La to Lu in apatite of the Hegau ijolite (Fig. 12d).

4.2.5. *Lileyite and wadeite*

Lileyite ($Ba_2(Na,Fe,Ca)_3MgTi_2(Si_2O_7)_2O_2F_2$), a sorosilicate of the lamprophyllite group was found in the Urach ijolite (EPMA results given in Table 4). Small amounts of Ti are substituted by Zr, Al, and V, while Ba may be partly replaced by K and Ca. Iron is accompanied by Mn; the REE concentrations are low and often subchondritic. The normalized pattern shows a maximum enrichment in the lightest and heaviest REE (La, Yb and Lu), progressively decreasing towards Nd, except for Eu, showing a strong positive anomaly (Eu/Eu* = 45–60; Fig. 12e).

Likewise, the cyclosilicate wadeite ($K_2ZrSi_3O_9$) occurs only in the Urach ijolite (EPMA results given in Table 5). Minor quantities of K and Zr are substituted by Ba and by Ti and Fe, respectively.

5. Discussion

5.1. *Ijolitic and nepheline syenitic domains represent differentiates of their host rocks*

The coarse-grained domains of all three investigated occurrences have an irregular shape and merge into the volcanic host rock in the form of a narrow contact zone in terms of their mineral composition and microstructure, without signs of reaction or resorption textures that would indicate disequilibrium between the two lithologies (Fig. 2b, c, g). The Hegau ijolite usually forms cm-sized pockets or lenses (Fig. 2a) and rarely veinlets, while the Urach ijolite occurs in a network of cm-sized veins or mm-thin veinlets, sometimes along former fractures generated during emplacement and cooling (Fig. 2c). The Kraichgau nepheline syenite typically appears as swarms of mm- to cm-thick, irregular veins.

Both ijolites and their melilititic–nephelinitic host rocks are devoid of feldspar and contain clinopyroxene, nepheline, titanomagnetite, apatite, and perovskite, albeit in varying quantities (Fig. 2b, d, e).

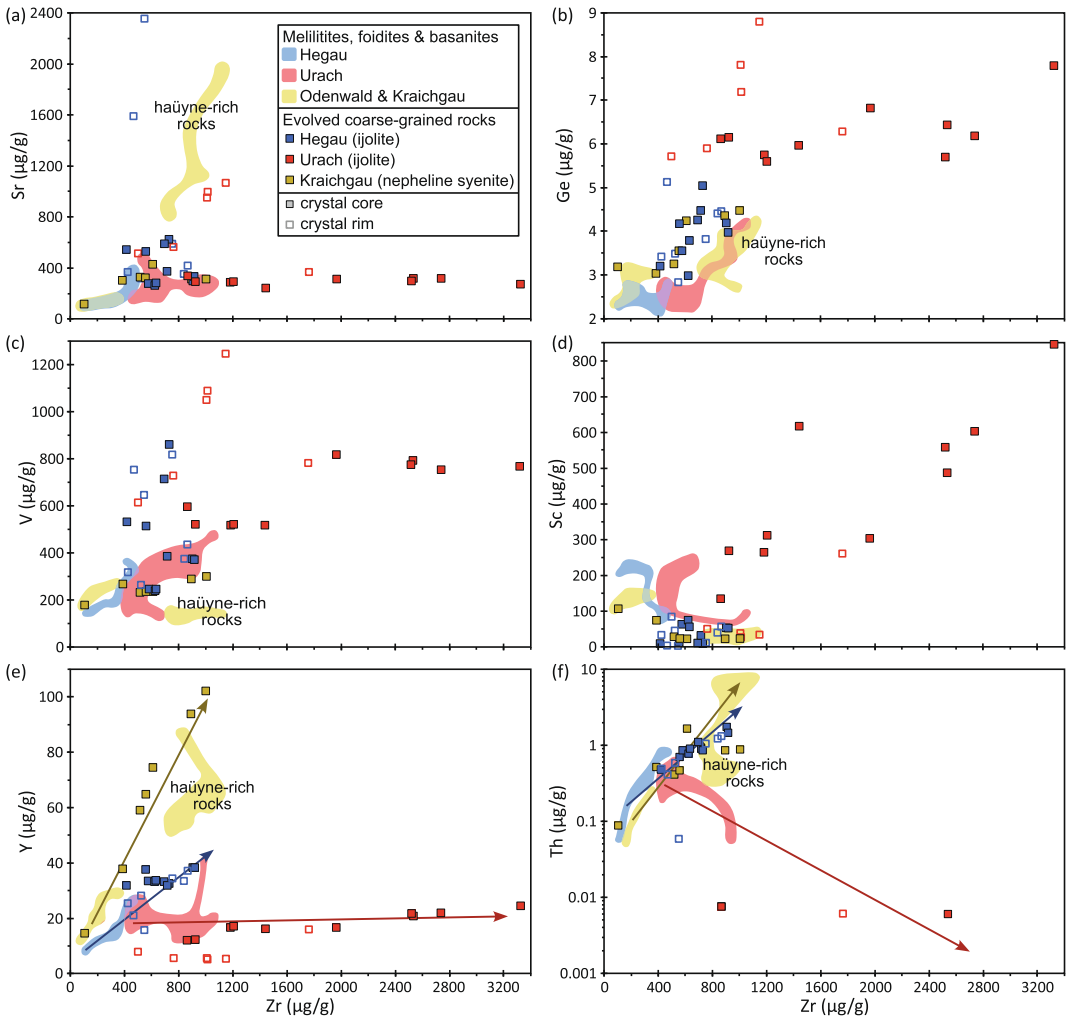

Fig. 6. Trace element composition of clinopyroxene in the investigated igneous rocks. Arrows are intended as a visual guide for the eyes and based on the changes in the measured compositions. Solid squares represent crystal cores and empty squares crystal rims. Zr vs. (a) Sr, (b) Ge, (c) V, (d) Sc, (e) Y, and (f) Th.

However, the ijolites lack olivine, melilite, and phlogopite and instead have higher nepheline, apatite, and perovskite contents (Fig. 3a-f). Similarly, the Kraichgau nepheline syenite contains more alkali feldspar, nepheline, and apatite, but no olivine and plagioclase and significantly smaller amounts of phlogopite, titanomagnetite, and clinopyroxene compared to its host phlogopite-nepheline basanite (Figs. 2f, g and 3g, h). All these features mirror an evolution with decreasing MgO, FeO, and CaO and increasing alkali, SiO_2, Al_2O_3, TiO_2 and P_2O_5 contents as well as decreasing Na/K ratios. Titanite instead of perovskite (Fig. 3i), and higher phlogopite contents in the nepheline syenite compared to the ijolites result from the different degrees of SiO_2-undersaturation, volatile contents, and Na/K ratios of the parental, melilititic–nephelinitic or phlogopite-nepheline basanitic melts.

This evolution is also reflected in the compositional changes of the minerals. The core compositions of clinopyroxene in the coarse-grained rocks largely resemble those of clinopyroxene in the host rocks (Fig. 5). In the crystal rims, however, hedenbergite and aegirine components are higher than in clinopyroxene of the primitive host rocks (Fig. 5b). The considerable variation in the three differentiation trends in terms of hedenbergite can be attributed to differences in the Mg/Fe ratio and/or oxygen fugacity (fO_2) of the melts at the time of late magmatic clinopyroxene crystallization. Since the melilititic host rock from Urach has a significantly higher Mg/Fe ratio (X_{Mg} = 0.78) than the melilite-bearing nephelinitic one from the Hegau (X_{Mg} = 0.70–0.72; Alibert et al., 1983; Hegner et al., 1995; Keller et al., 1990; Krause and Weiskirchner, 1981; Walter, 1994), this could explain the lower proportion of hedenbergite in the Urach ijolite compared to the Hegau ijolite. In contrast, the low Mg/Fe ratio in the host rocks of the Kraichgau nepheline syenite (X_{Mg} = 0.50–0.53; Binder et al., 2024a) excludes the same cause for the more direct evolution of these melts to aegirine-rich compositions, as it would favour hedenbergite-rich compositions. Rather, the higher fO_2, which shifts Fe in the melt towards ferric species, may be responsible for this effect, consistent with very high fO_2 determined for the evolved haüyne-rich rocks in the same region, which contain very hedenbergite-poor aegirine, continuing the differentiation trend of the nepheline syenite (Fig. 5b; Mann et al., 2006, Binder et al., 2024a).

Low Al and Ti contents at decreasing X_{Mg} in clinopyroxene rims in the ijolites correspond to decreasing Tschermak and diopside components and increasing proportions of aegirine (Fig. 5a-d). These features reflect the increase in alkali content and silica activity ($aSiO_2$) during melt evolution, the Ti depletion from titanomagnetite and perovskite fractionation, and the preferential incorporation of Al into cogenetic nepheline. The same effect is observed for the haüyne-rich rocks of the Odenwald and Kraichgau area. However, their Ti aegirine component in clinopyroxene crystallized during the late magmatic stage is higher, possibly indicating less prior Ti extraction by titanomagnetite and titanite fractionation.

Most trace element concentrations in clinopyroxene (e.g., Li, Sr, Ga, Ge, V, Sc, Y, Zr, Th, REE, Hf, Nb, Ta) in the ijolites and nepheline syenite partially overlap with those in clinopyroxene of the primitive host rocks

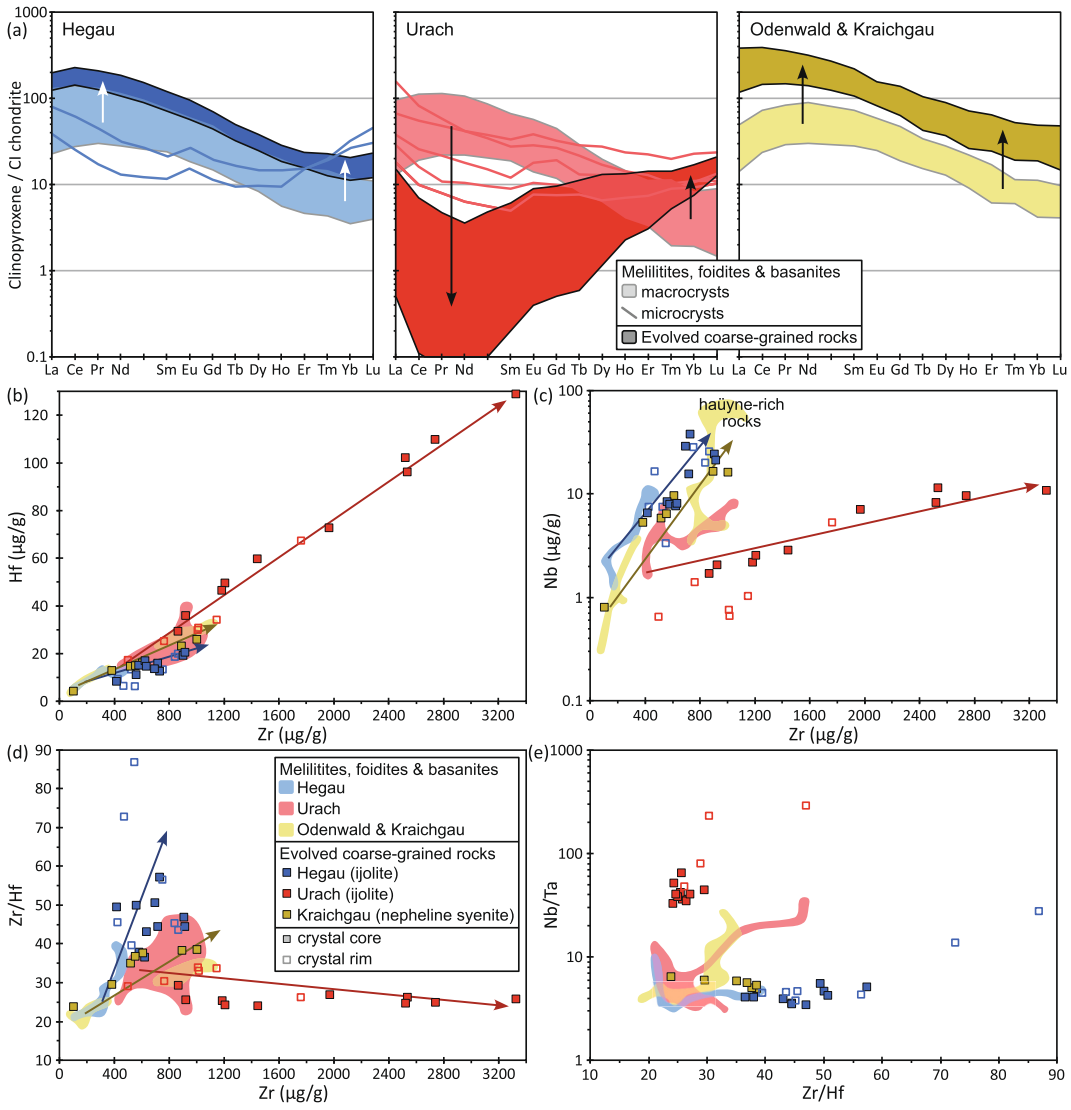

Fig. 7. Trace element composition of clinopyroxene in the investigated igneous rocks. Arrows are intended as a visual guide for the eyes and based on the changes in the measured compositions. Solid squares represent crystal cores and empty squares crystal rims. (a) Chondrite-normalized REE patterns of clinopyroxene in the ijolites and the nepheline syenite compared with those of clinopyroxene macrocrysts and microcrysts from the primitive host rocks of the same regions (normalization values from Palme and O'Neill, 2014). Zr vs. (b) Hf, (c) Nb, and (d) Zr/Hf. (e) Zr/Hf vs. Nb/Ta.

and/or directly follow their evolutionary trend with variable trajectories (Figs. 6 and 7; Supplementary material, Fig. A2a-e). This is also observed for Ti, Mn, Zn, and V contents in the Fe—Ti oxides (Fig. 8), for Nb, Ta, Na, Sr, Ba, Fe, Th, U, Y, and Pb in perovskite (Figs. 9 and 10; Supplementary material, Fig. A3a, b), and for F, Cl, S, V, Na, Sr, and REE in apatite (Fig. 12; Supplementary material, Fig. A1). Altogether, mineral proportions, assemblages, and compositions imply that the ijolites and the nepheline syenite are differentiation products of their primitive host rocks, comparable to observations in a melilite nephelinite from the Eger Graben system (Ulrych et al., 2000). Hegau ijolite and Kraichgau nepheline syenite provide missing links in the differentiation trajectory from melilititic–nephelinitic magmas towards nosean phonolites in the Hegau and nepheline basanites towards haüyne-rich rocks in the Odenwald and Kraichgau region (Binder et al., 2024b; Mann et al., 2006).

5.2. *P-T conditions during melt separation*

The mineral assemblages of the ijolites and the nepheline syenite prove that the separation of small amounts of residual melt happened after crystallization of olivine ± melilite but during co-precipitation of clinopyroxene, titanomagnetite, and nepheline. Accordingly, the coarse-grained rocks represent the only visible differentiation stage within the three volcanic edifices, albeit at a time when the magma was already perceptibly evolved. Nevertheless, the ijolites and the nepheline syenite show that melt separation and further evolution in a subsystem occur on a small-volume scale even in quickly ascending and cooling magmas of primitive, alkaline, SiO_2-undersaturated composition.

Clinopyroxene-based geothermobarometry (Neave and Putirka, 2017; Eq. 33 in Putirka, 2008; Supplementary material, File 1) applied to the volcanic host rocks yields crystallization pressures (*P*) and temperatures (*T*) of 430–770 MPa and 1180–1220 °C (Hegau), 0–810 MPa and 1200–1300 °C (Urach), and 0–820 MPa and 1110–1200 °C (Kraichgau). The estimates are slightly lower when considering whole-rock H_2O contents (410–770 MPa at 1160–1220 °C, 0–700 MPa at 1150–1260 °C, and 0–800 MPa at 1090–1180 °C, respectively; Supplementary material, Fig. A4a, b). These *P-T* estimates represent the possible minimum and maximum values during separation of the ijolitic or nepheline syenitic residual melts, formed within the crystallization interval of clinopyroxene in their host rock.

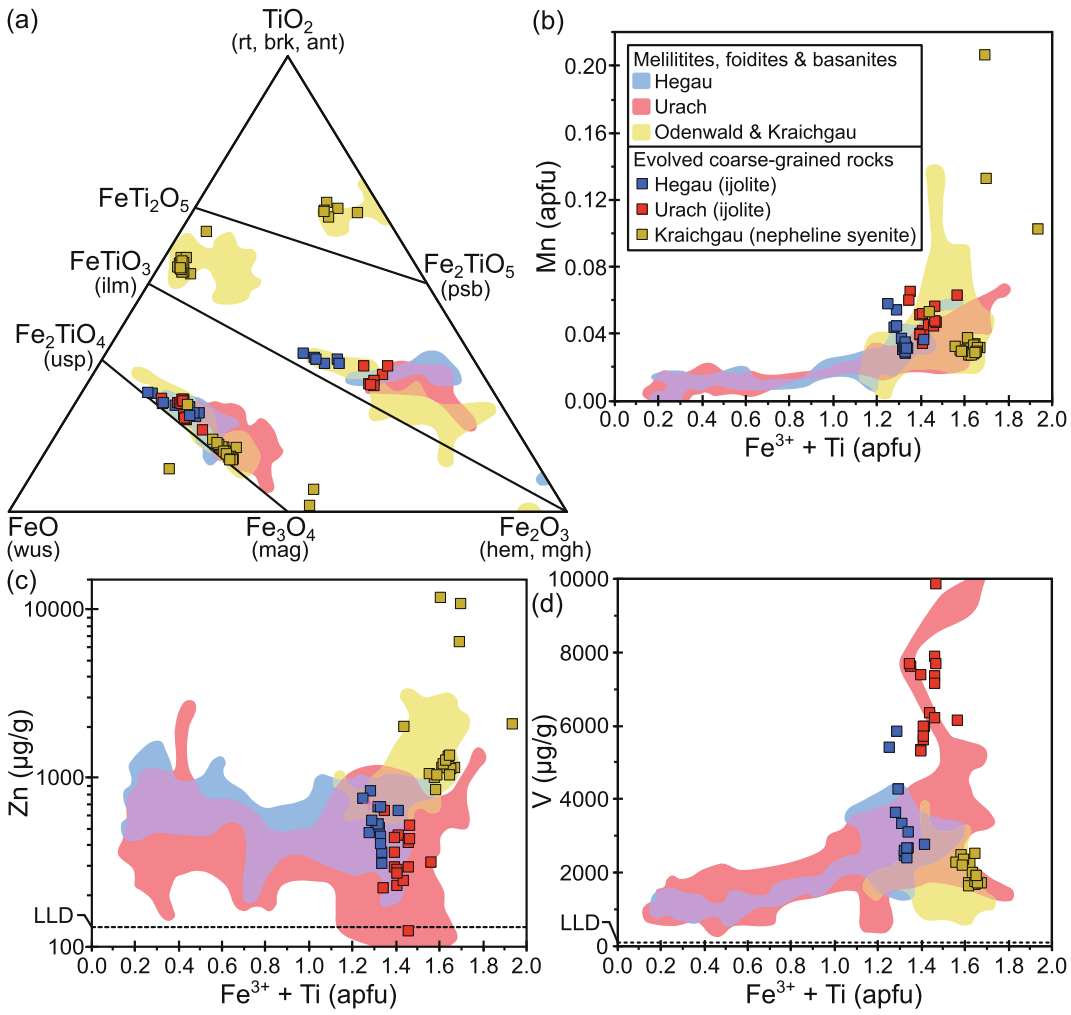

Fig. 8. Fe—Ti oxide composition in the investigated igneous rocks. EPMA data of this work is supplemented by Binder et al. (2024a, 2024b), Mann et al. (2006), and Stähle and Koch (2003). (a) Triangular diagram based on Fe—Ti and (Fe,Ti)-O ratio. Many data points plot along magnetite–ulvöspinel$_{ss}$ (titanomagnetite) but may be shifted towards hematite/maghemite because of alteration and weathering. Ilmenite in the Odenwald and Kraichgau rocks reflects exsolution lamellae in euhedral titanomagnetite macrocrysts. The occurrence of Ti-rich hematite with unclear stoichiometry is due to exclusion of other cations in the plot (e.g., Mg, Mn, Al). Pseudobrookite is restricted to localities in the Odenwald and Kraichgau region and slightly off the ideal solid solution series between pseudobrookite and ferro-pseudobrookite due to the incorporation of Mg, Mn, Al, V, Zr, and Nb. Fe^{3+}+Ti vs. (b) Mn, (c) Zn, and (d) V. apfu – atoms per formula unit; LLD – lower limit of detection.

Clinopyroxene-only geothermobarometry (Eqns. 32a, b in Putirka, 2008; Eqns. 32b and 32dH in Wang et al., 2021) applied to the coarse-grained domains is subject to various uncertainties and shows a wide range for crystallization *P* (~0–600 MPa for the ijolites, ~0–1000 MPa for the nepheline syenite; Supplementary material, File 1). Depending on the assumed H_2O content of the melt, the determined crystallization *T* (850–1090 °C) differ, but show large variations irrespective of this (Supplementary material, Fig. A5), which is to be expected in a rapidly cooling magmatic system emplaced close to the surface. Although a precise determination is difficult, the results imply that melt separation at all three localities occurred at crustal depths between the emplacement level and a maximum of 30 km (~800 MPa). This indicates a direct temporal relationship with magma ascent and eruption, since the coarse-grained domains are clearly differentiation products of their mantle-derived host magmas. However, unlike fractional crystallization in larger magma chambers, such differentiation processes do not involve effective crystal-melt separation, so that neither self-sustaining and progressive differentiation towards phonolitic compositions nor significant amounts of cumulates are observed.

5.3. *Variable enrichment and distribution of incompatible trace elements and volatiles*

In this chapter, differences and similarities between the ijolitic and nepheline syenitic domains are discussed in relation to mineral and chemical composition of the respective host magmas.

5.3.1. *Factors controlling the composition of the ijolites*

The primitive melilititic–nephelinitic parental melts of the Hegau and Urach ijolites first underwent fractionation of olivine and oxyspinel, followed by melilite, clinopyroxene, perovskite, and nepheline (Binder et al., 2024a). This sequential fractionation process can only explain the uniform and continuous geochemical trends in both ijolites, like the enrichment of incompatible and depletion of compatible elements relative to the parental melts, as seen in clinopyroxene (e.g., Mg, Al, Zr, V, Li, Ga; Figs. 5 and 6c, Supplementary material, Fig. A2a, b), titanomagnetite (e.g., Mn, V; Fig. 8b, d), and perovskite (e.g., Fe; Fig. 9f). The following section addresses the different onset of separation of the ijolitic residual melts from the Hegau and Urach regions and the initially small but diverging compositional variations of the two parental host magmas. Together, these factors caused large differences between the

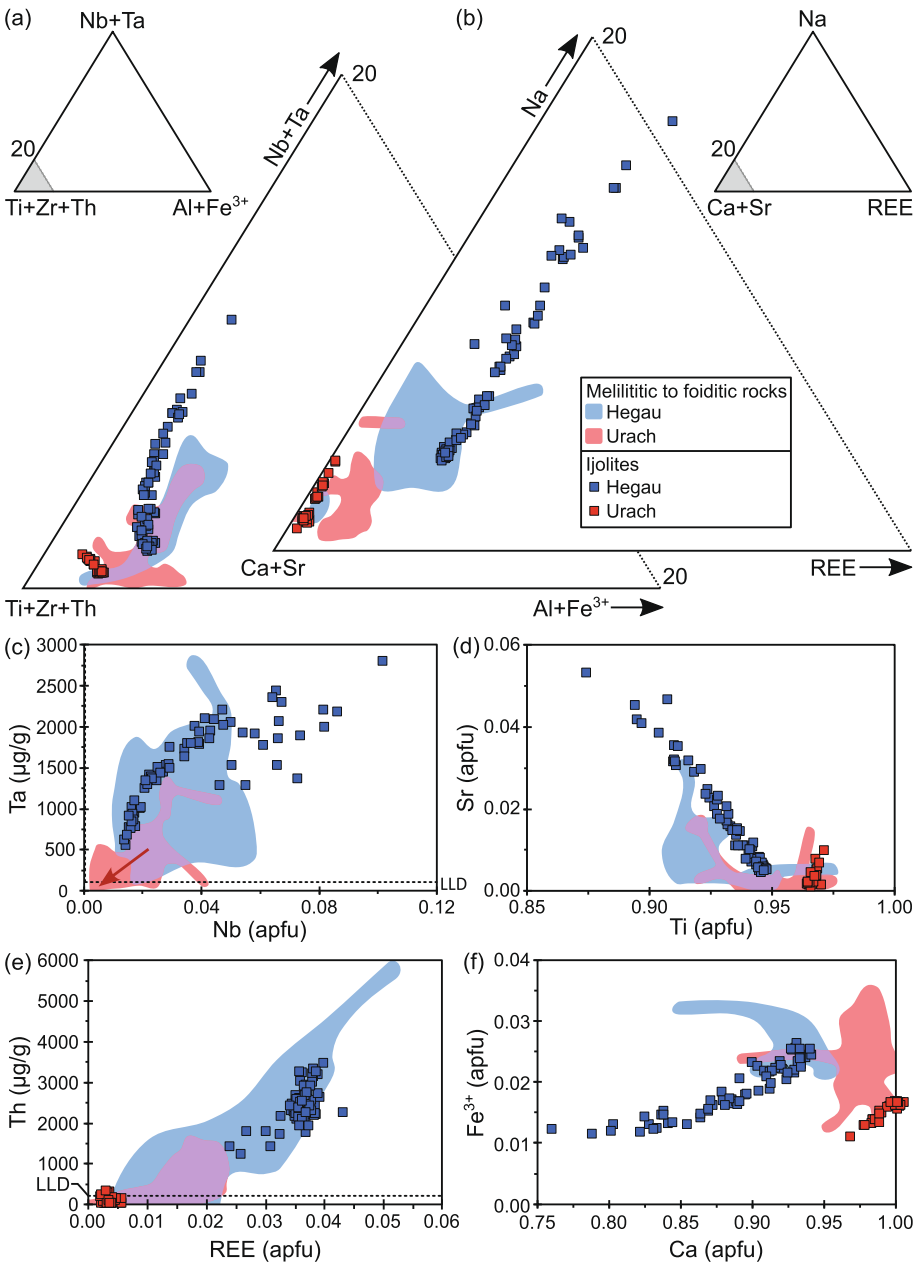

Fig. 9. Perovskite composition in the investigated igneous rocks. EPMA data of this work is supplemented by Binder et al. (2024a, 2024b). Triangular diagrams showing (a) the molar Nb + Ta – Ti + Zr + Th – Al + Fe^{3+} and (b) the Na–REE–Ca + Sr distribution normalized to 100 %. (c) Nb vs. Ta. Note that Ta concentrations in perovskite of the Sternberg ijolite are all below the detection limit. (d) Ti vs. Sr, (e) REE vs. Th, and (f) Ca vs. Fe^{3+}. apfu – atoms per formula unit; LLD – lower limit of detection.

two coarse-grained domains in the incompatible element patterns of various minerals, notwithstanding their derivation from strikingly similar parental melts, particularly regarding trace element concentrations (Binder et al., 2024a).

The Hegau ijolite contains abundant skeletal perovskite and titanomagnetite, indicating their rapid growth under a high degree of supersaturation of corresponding elements (Ca, Ti and/or Fe) due to rapid undercooling (Fig. 3b, c; Gornitz, 1981). During crystallization, large quantities of trace elements reasonably compatible with perovskite and/or oxyspinel were removed promptly from the residual melt, in particular Mn, V, Nb, Ta, Na, Sr, Ba, Th, REE, and U (Figs. 8b, d, 9 and 10a-c). Abundant euhedral fluorapatite crystals also formed early in the ijolite (Fig. 3a) and, compared to those in the primitive volcanic rocks, they are Cl- and H_2O-enriched but slightly depleted in F (Fig. 12a). Likewise, clinopyroxene (which crystallized slightly later) shows a significant enrichment of incompatible trace elements (especially Sr, Y, Th, REE, Nb, Ta) compared to clinopyroxene in the host rock and relative to clinopyroxene in the Urach ijolite (Figs. 6a, e, f and 7a, c; Supplementary material, Fig. A2c-e). This is consistent with the evolution of an increasingly volatile- (F, Cl, H_2O), HFSE-, LILE-, and REE-enriched alkaline magma.

The residual ijolitic melt from Urach exhibits a markedly different evolutionary path compared to that from the Hegau, although euhedral apatite, perovskite, and titanomagnetite also crystallized early, yet without pronounced skeletal growth and accordingly more slowly (Fig. 3d-f). Perovskite in the Urach ijolite has low Nb, Ta, Na, Sr, Ba, Th, LREE, Pb, and U contents and, relative to perovskite in the primitive volcanic host rocks, shows no enrichment in these elements or even significantly lower contents (Figs. 9 and 10a-c, h; Supplementary material, Fig. A3b). Clinopyroxene is strongly depleted in LREE, Th, and Ta

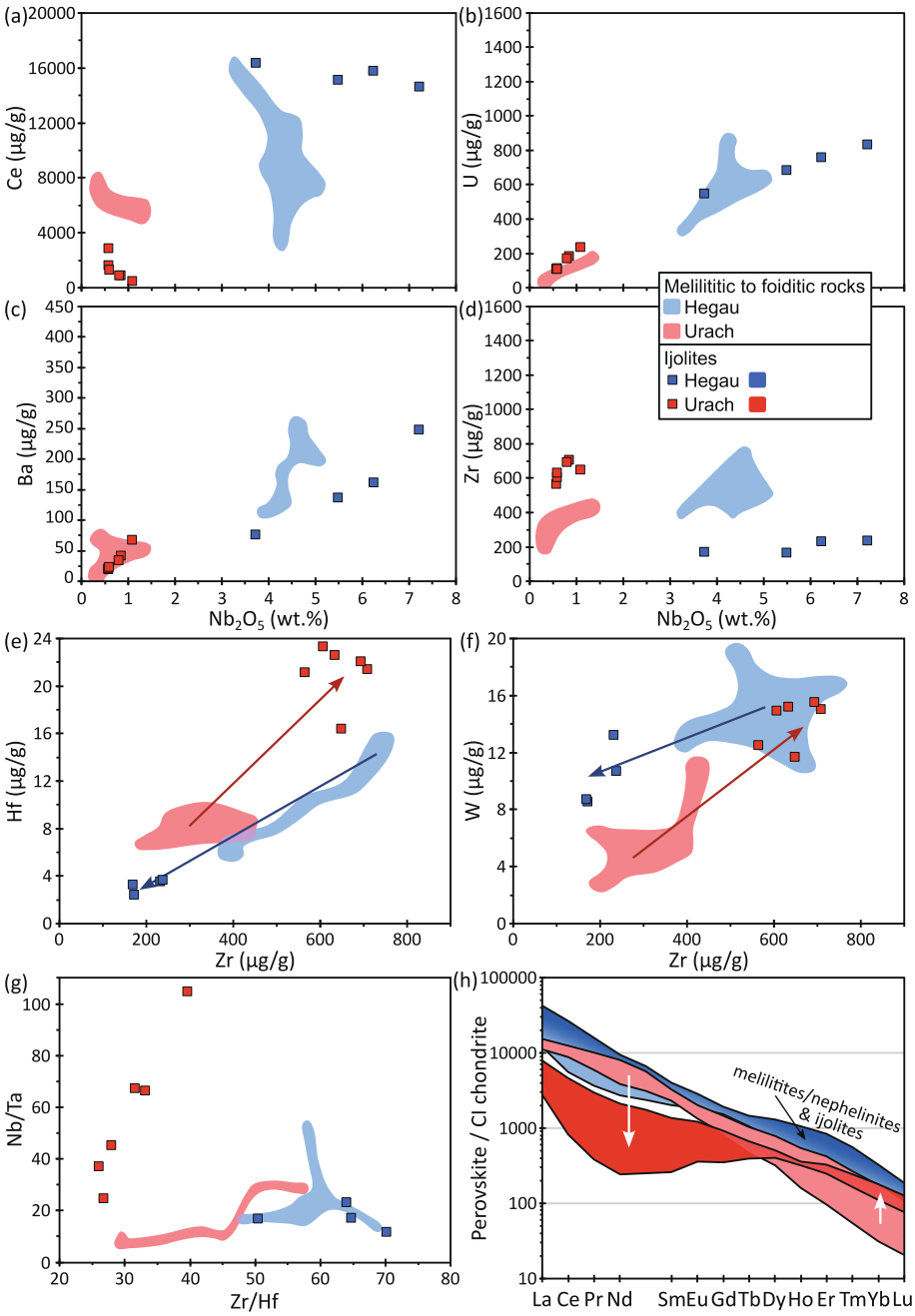

Fig. 10. Trace element composition of perovskite in the investigated igneous rocks. Arrows are intended as a visual guide for the eyes and based on the changes in the measured compositions. Nb_2O_5 vs. (a) Ce, (b) U, (c) Ba, and (d) Zr. (e) Zr vs. Hf and (f) vs. W. (g) Zr/Hf vs. Nb/Ta. (h) Chondrite-normalized REE patterns of perovskite.

(Figs. 6f and 7a, e), and its concentrations of Sr, Y, and Nb are comparable to those found in clinopyroxene from the melilititic–nephelinitic rocks, but on average markedly lower than those in clinopyroxene from the Hegau ijolite (Figs. 6a, e and 7c). Further, fluorapatite has lower REE concentrations in the Urach ijolite than in the Hegau ijolite (Supplementary material, Fig. A1). All these compositional and textural differences indicate that the residual melt, in contrast to that of the Hegau ijolite, was less enriched or already depleted in numerous incompatible elements at the time of its separation. However, this does not apply to Zr, Hf, and W, which have significantly higher concentrations in perovskite and clinopyroxene from the Urach ijolite than in the same minerals from the Hegau ijolite and the primitive host rock (Figs. 7b and 10d-f), suggesting previous fractionation processes that separated these three from most other trace elements.

The chondrite-normalized REE pattern of clinopyroxene from the Urach ijolite continues an evolutionary trend observed in microcrysts in the primitive melilititic–nephelinitic rocks from Urach and the Hegau region (Fig. 7a). This indicates that separation of the ijolitic melt in the case of Urach occurred, when the crystallization of groundmass phases (i.e., perovskite, titanomagnetite, clinopyroxene microcrysts) had already initiated. The ijolitic residual melt was thus strongly depleted in LREE from the beginning, which explains the marked troughs in REE patterns of clinopyroxene (Fig. 7a) and perovskite (Fig. 10h). In contrast, the residual melt producing the Hegau ijolite probably separated at an earlier stage, when clinopyroxene crystallization in the host magma was less advanced and perovskite formation had not yet begun. The REE patterns of clinopyroxene and perovskite are not significantly different from those in the melilitic–nephelinitic Hegau rocks, except for

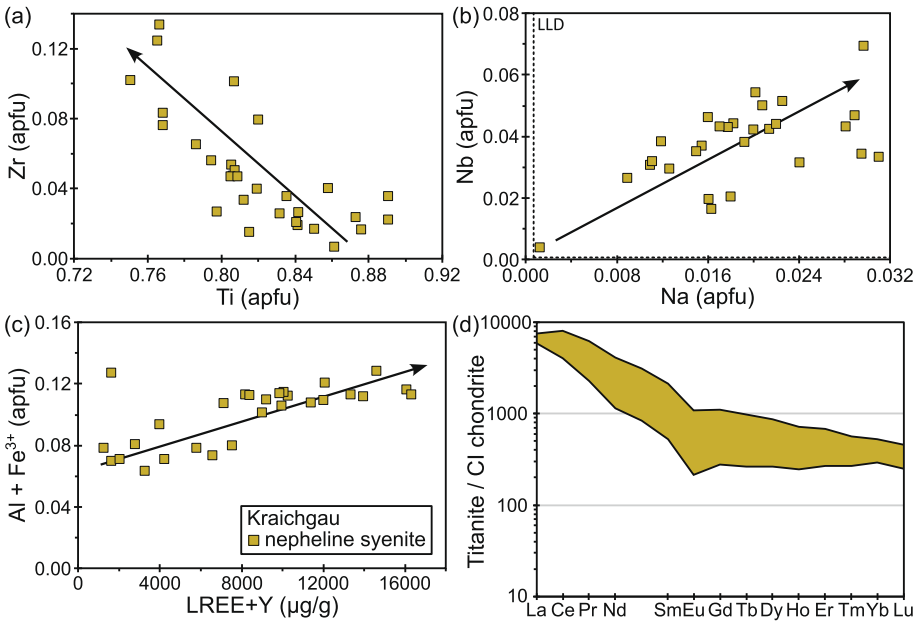

Fig. 11. Titanite composition (EPMA) in the nepheline syenite from the Steinsberg. Arrows are intended as a visual guide for the eyes and based on the changes in the measured compositions. (a) Ti vs. Zr, (b) Na vs. Nb, (c) LREE+Y vs. Al + Fe^{3+}, and (d) chondrite-normalized REE pattern of titanite (LA-ICP-MS; normalization values from Palme and O'Neill, 2014); apfu – atoms per formula unit; LLD – lower limit of detection.

the higher enrichment factors, confirming that the residual melt was still REE-rich.

Titanomagnetite and perovskite have $D_{Nb/Ta} < 1$, and the absolute values for D_{Nb}, D_{Ta}, and D_{Th} are above 1 for one or both minerals (Kato et al., 1988; Nielsen, 1992). Hence, separation of the ijolitic melt during progressive titanomagnetite and perovskite crystallization in the Urach case is in agreement with the low contents of Nb, Ta, and Th and with the high Nb/Ta ratios in clinopyroxene and perovskite of the coarse-grained residue (Figs. 6f, 7c, e, 9c, e and 10g). In contrast, the skeletal habit of perovskite and titanomagnetite in the Hegau ijolite shows that Ca, Ti, and/or Fe saturation in the parental magma was still very high at the time of melt separation, indicating that crystallization of the two minerals was in its initial stage. This accounts for higher Nb, Ta, and Th concentrations and lower Nb/Ta ratios in clinopyroxene and perovskite. However, no magmatic mineral phase that crystallized in the host rocks is capable of effectively depleting the melt in Zr, Hf, and W during magmatic evolution prior to the formation of the ijolitic residual melts (e.g., Adam and Green, 2006; Ambrosio and Azzone, 2018; Kuehner et al., 1989). A small volume of residual melt separated at a later stage would therefore be particularly enriched in these elements. Consequently, Zr, Hf, and W have significantly higher concentrations in clinopyroxene and perovskite in the Urach ijolite than in the Hegau ijolite, whose relevant melt separated earlier.

Although D_{Zr}^{Cpx} and D_{Hf}^{Cpx} in alkaline magmas are <1 to ≈1, clinopyroxene fractionates Zr from Hf in such systems as $D_{Zr/Hf}$ is always <1 (Adam and Green, 2006; Ambrosio and Azzone, 2018; Minissale et al., 2019). Thus, the significantly lower modal abundance of clinopyroxene relative to melilite in the primitive rocks of the Urach locality, compared to those from the Hegau site, accounts for the lower Zr/Hf ratios in clinopyroxene and perovskite in the Urach ijolite (Figs. 7d, e and 10g). Likewise, the lower Sr enrichment of perovskite in the ijolitic residual melt reflects higher modal amounts of highly Sr-compatible melilite in the primitive Urach rocks (Fig. 6a). The difference in the clinopyroxene-to-melilite ratio between the host rocks is also relevant for Ge and Sc concentrations in the ijolites: both elements are less compatible for melilite than for the more SiO_2-rich phase clinopyroxene (Adam and Green, 2006; Beckett et al., 1990; Minissale et al., 2019; Nagasawa et al., 1980), causing their higher concentrations in clinopyroxene of the Urach ijolite (Fig. 6b, d).

Rayleigh fractional crystallization modelling based on Sr—Sc systematics in clinopyroxene indicates that, in the Hegau case, fractionation of ~50–85 % clinopyroxene and melilite from the melt – in a ratio between 75:25 and 100:0, starting from the onset of clinopyroxene crystallization in the host rock – predicts compositions matching those observed in clinopyroxene from the ijolite (Fig. 13a). Replicating the clinopyroxene compositions in the Urach ijolite instead requires prior removal of larger amounts of clinopyroxene and melilite (~70–92 % since the onset of clinopyroxene crystallization in the host), with modal ratios of ~35:65 to ~65:35. The latest crystal rims in both ijolites formed after ~94–97 % crystal extraction, clinopyroxene dominating over melilite in the final stages of fractionation according to the model (Fig. 13b), consistent with the absence of melilite in the two ijolites. The findings confirm both the greater extent of melilite fractionation in the parental Urach melt and a delayed melt separation compared to the Hegau case.

In summary, earlier melt separation at the beginning of perovskite crystallization and prior to the end of clinopyroxene macrocryst formation at a high clinopyroxene-to-melilite ratio during fractionation in the host melt (Hegau) led to an enrichment of almost all incompatible trace elements in the ijolite. Later separation (towards the end of clinopyroxene and perovskite crystallization) in a more melilite-rich magma (Urach) affected particularly the REE and HFSE budget and is reflected in high Ge and Sc, but low Sr concentrations as well as high Nb/Ta and Zr/Nb, but low La/Lu and Zr/Hf ratios in ijolite-hosted clinopyroxene and perovskite.

5.3.2. *Late-stage formation of agpaitic assemblages in the Urach ijolite*

At the final stages of the ijolitic melt evolution at Urach, lileyite, wadeite, and Sr-enriched apatite crystallized (Fig. 4), implying F-, LILE- and Zr-enriched, relatively SiO_2-poor and peralkaline residual melts with low Na/K ratios, with striking parallels to agpaitic systems (cf. Marks and Markl, 2017). Hydrous melts or aqueous fluids, however, seem to have played a negligible role, considering that no hydrous minerals formed during these final stages. Presumably, the H_2O contents of the parental melt were already very low, as evidenced by the very small amounts of hydrous minerals in the host rock, which are moreover mostly F-dominated (fluorophlogopite, fluorokinoshitalite, fluorapatite; Binder et al., 2024a). Further, Sr and Ba appear to have been enriched

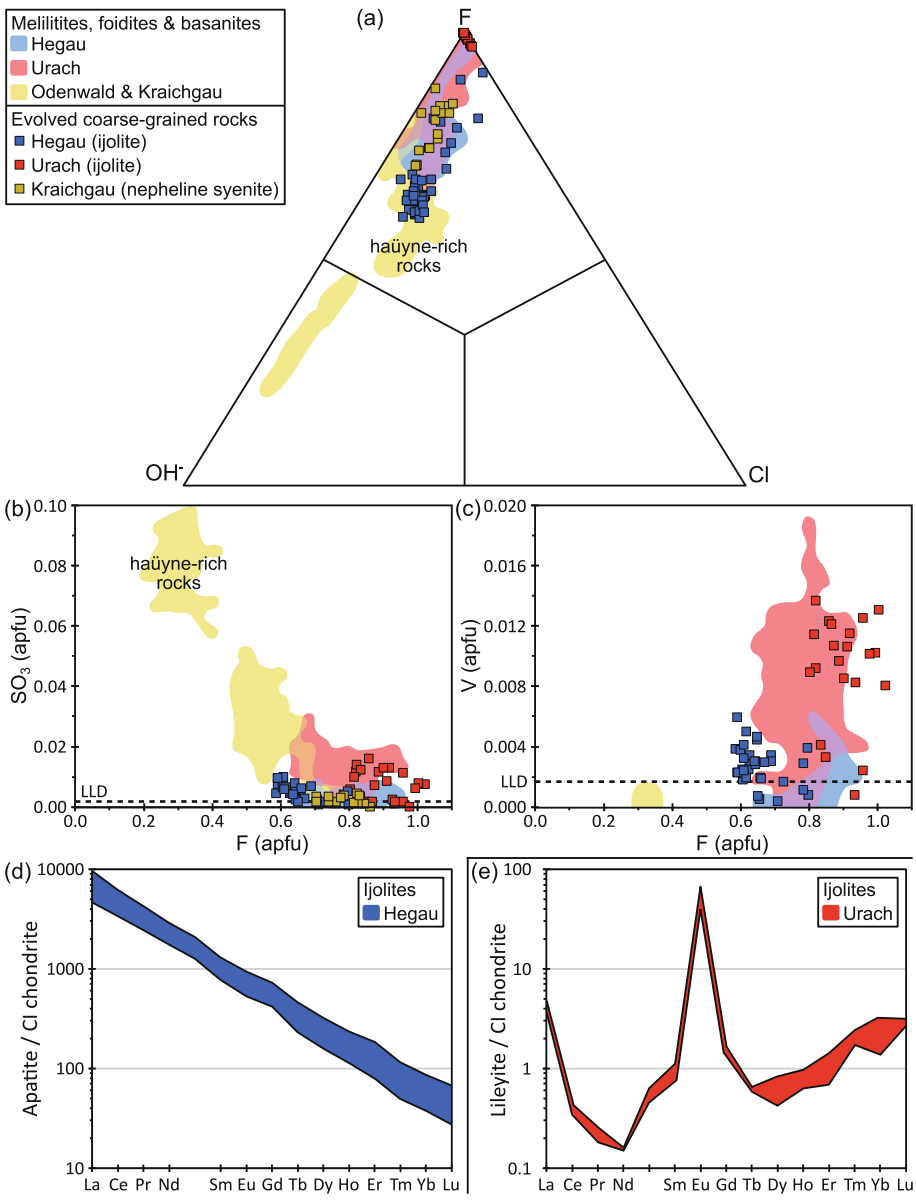

Fig. 12. (a-d) Apatite composition in the investigated igneous rocks. EPMA data of this work is supplemented by Binder et al. (2024a, 2024b). (a) Triangular classification diagram based on the anion position (OH^-, F, Cl). F vs. (b) SO_3 and (c) V; apfu – atoms per formula unit; LLD – lower limit of detection. Chondrite-normalized REE patterns of (d) apatite and (e) lileyite in the ijolites (LA-ICP-MS; normalization values from Palme and O'Neill, 2014).

only at the very end of residual melt evolution: initially, both were more concentrated in the ijolitic Hegau melt than in that from Urach (Figs. 6a, 9d, and 10d), but in the latter, skeletal perovskite crystallization did not occur early, preventing depletion of these elements.

The pronounced enrichment of K relative to Na in the highly evolved residual melt, derived from an originally sodic, alkaline, and strongly SiO_2-undersaturated parental magma, is primarily due to fractionation of Na-bearing but K-free melilite (alumoåkermanite component) and clinopyroxene (aegirine component). The increase in K is further reflected by the occurrence of kalsilite in the groundmass of olivine melilitites from Urach (Binder et al., 2024). Aluminium depletion begian during clinopyroxene crystallization (via Al Tschermak) in the volcanic host and continued with the formation of nepheline in both the groundmass and the ijolite (Fig. 3).

The high F concentrations in the Urach ijolite are indicated by the abundance of fluorapatite (Fig. 3d-f), which, unlike that in the Hegau ijolite, has a pure F endmember composition (Fig. 12a). Fluorine plays a key role in retaining HFSE in residual melts (Andersen et al., 2010; Giehl et al., 2014), mirrored in the absence of Zr-rich mineral phases in the host rock. This culminated in the crystallization of an agpaitic assemblage composed of lileyite, wadeite, and Sr-rich fluorapatite. The positive Eu anomaly in lileyite (Fig. 12e) results from the compatibility of Eu^{2+} in this mineral, where it substitutes for Ba and Ca, whereas the trivalent REE display incompatible behaviour.

5.3.3. *Petrogenesis of the nepheline syenite*

Setting aside the compositional differences between the host rocks, the magmatic evolution of the nepheline syenite emplaced in the phlogopite-nepheline basanite from the Kraichgau region resembles that of the Hegau ijolite. The separation from the parental melt occurred during the crystallization of clinopyroxene, phlogopite, nepheline, and feldspars (predominantly plagioclase) but after olivine fractionation and during the waning stages of titanomagnetite precipitation. Despite counteracting phlogopite fractionation, crystallization of plagioclase, nepheline and aegirine-bearing clinopyroxene in the host rock obviously caused an increase in the Na/K ratio in the nepheline syenitic residual

Table 4
Representative EPMA analyses of lileyite from Sternberg volcano (Urach). Mineral formulas were calculated based on 18 oxygen and 12 cations with correction for Fe^{3+}.

Analysis	U001–7	U001–17	U001–18	U001–20	U001–21	U001–26	U001–29	U001–43	U001–44	U001–45	U001–48	U001–55
wt%												
SiO_2	28.24	28.29	28.73	28.43	28.49	28.45	28.07	28.70	28.46	28.26	28.50	28.55
TiO_2	19.77	17.27	21.27	19.38	20.19	19.86	17.10	19.12	18.25	16.89	20.37	17.57
ZrO_2	0.80	0.07	0.80	0.13	0.88	0.15	0.30	0.23	0.56	0.13	0.84	0.23
Al_2O_3	0.15	0.16	0.11	0.21	0.16	0.20	0.16	0.26	0.11	0.17	0.19	0.19
V_2O_3	0.12	0.02	0.19	0.11	0.11	0.12	–	0.16	0.14	–	0.10	0.04
Cr_2O_3	0.02	–	–	–	–	–	0.01	–	–	–	–	–
Fe_2O_3	1.46	0.07	1.10	1.28	1.24	1.08	0.39	0.26	0.92	0.06	0.12	3.69
FeO	3.24	7.60	2.53	3.40	2.92	4.61	7.50	5.37	6.10	8.70	4.28	4.40
MnO	0.46	0.73	0.37	0.47	0.39	0.58	0.64	0.51	0.63	0.81	0.47	0.66
MgO	4.63	5.89	3.85	5.19	4.20	4.88	5.55	5.04	5.12	5.80	4.44	5.80
CaO	2.53	2.34	2.08	2.80	2.15	2.61	2.21	2.68	2.29	2.35	2.25	2.46
BaO	27.40	27.05	26.78	27.50	27.57	26.27	27.26	27.10	26.47	26.89	27.00	26.10
ZnO	0.02	0.02	0.00	–	–	0.02	–	0.03	0.02	0.01	–	–
Na_2O	7.57	5.93	8.25	7.26	7.77	7.47	6.15	7.03	6.73	5.84	7.67	6.55
K_2O	1.36	1.12	1.69	1.32	1.43	1.42	1.08	1.33	1.38	1.16	1.44	1.26
F	4.05	4.24	3.82	4.18	3.73	4.38	4.32	4.22	4.20	4.50	4.02	3.95
Cl	–	–	–	–	0.01	–	–	0.02	–	0.01	0.02	–
$–O=F_2$	1.71	1.79	1.61	1.76	1.57	1.84	1.82	1.78	1.77	1.89	1.69	1.66
Total	**100.1**	**99.00**	**99.96**	**99.90**	**99.68**	**100.3**	**98.92**	**100.3**	**99.62**	**99.67**	**100.0**	**99.78**
apfu												
Si^{4+}	3.998	4.073	4.043	4.019	4.053	3.987	4.058	4.047	4.050	4.050	4.028	4.032
Ti^{4+}	2.105	1.870	2.251	2.060	2.160	2.093	1.859	2.028	1.953	1.820	2.165	1.866
Zr^{4+}	0.055	0.005	0.055	0.009	0.061	0.011	0.021	0.016	0.039	0.009	0.058	0.016
Al^{3+}	0.024	0.027	0.018	0.035	0.027	0.033	0.028	0.043	0.019	0.028	0.031	0.031
V^{3+}	0.014	0.002	0.021	0.012	0.013	0.014	–	0.018	0.016	–	0.011	0.005
Cr^{3+}	0.002	–	–	–	–	–	0.001	–	–	–	–	–
Fe^{3+}	0.155	0.007	0.117	0.136	0.133	0.114	0.042	0.027	0.099	0.006	0.013	0.392
Fe^{2+}	0.384	0.915	0.298	0.402	0.347	0.540	0.907	0.633	0.726	1.043	0.506	0.520
Mn^{2+}	0.056	0.089	0.044	0.057	0.047	0.069	0.079	0.061	0.076	0.098	0.056	0.079
Mg^{2+}	0.977	1.264	0.808	1.094	0.891	1.020	1.196	1.060	1.086	1.239	0.935	1.221
Ca^{2+}	0.384	0.361	0.314	0.424	0.328	0.392	0.342	0.405	0.349	0.361	0.341	0.372
Ba^{2+}	1.520	1.526	1.477	1.524	1.537	1.443	1.544	1.498	1.476	1.510	1.495	1.445
Zn^{2+}	0.002	0.002	–	–	–	0.002	–	0.003	0.002	0.001	–	–
Na^{+}	2.078	1.655	2.251	1.990	2.143	2.030	1.724	1.922	1.857	1.623	2.102	1.794
K^{+}	0.246	0.206	0.303	0.238	0.260	0.254	0.199	0.239	0.251	0.212	0.260	0.227
Total	**12.00**	**12.00**	**12.00**	**12.00**	**12.00**	**12.00**	**12.00**	**12.00**	**12.00**	**12.00**	**12.00**	**12.00**
F^{-}	1.813	1.930	1.700	1.869	1.678	1.941	1.975	1.882	1.890	2.040	1.797	1.764
Cl^{-}	–	–	–	–	0.002	–	–	0.005	–	0.001	0.004	0.000
Total	**1.813**	**1.930**	**1.700**	**1.869**	**1.680**	**1.941**	**1.975**	**1.887**	**1.890**	**2.041**	**1.801**	**1.764**

– – below detection limit; apfu – atoms per formula unit.

melt, which led to an increasing dominance of alkali feldspar over plagioclase. The higher $aSiO_2$ and water activity (aH_2O) at lower F and P concentrations compared to the ijolitic melts are due to the differences between the host rocks (see Section 5.1) and resulted in the formation of OH-dominated phlogopite, and accessory titanite, but significantly less apatite and the absence of perovskite (Figs. 2g and 3g-i).

The enrichment of incompatible elements in the nepheline syenite compared to the host rock is mainly due to the relative enrichment in the residual melt by removal of compatible elements during fractional crystallization. This caused elevated concentrations of Sr, Ge, Th, Zr, Hf, Nb, Ta, and especially of REE + Y in clinopyroxene (Figs. 6a, b, e, f and 7a-c, Supplementary material, Fig. A2c-e) and of Mn and Zn in titanomagnetite (Fig. 8b, c). Titanite has exceptionally high Na, Al, Zr, Hf, REE, Nb, and Th concentrations (Fig. 11, Supplementary material, File 3). The slightly negative Eu anomaly in its REE pattern (Fig. 11d) results from early crystallization of plagioclase, which preferentially incorporates the Eu, present partly as Eu^{2+} over the remaining REE. Scandium depletion (Fig. 6d) is attributed to its compatibility for clinopyroxene (Adam and Green, 2006), which crystallized abundantly before separation of the nepheline syenitic melt.

5.3.4. *Composition of the ijolitic and nepheline syenitic residual melts*

Using the compositions of clinopyroxene in the coarse-grained domains and D^{Cpx} for evolved alkaline, SiO_2-undersaturated melts (Larsen, 1979; Villemant, 1988; Wörner et al., 1983), the composition of the residual melt in equilibrium with clinopyroxene can be estimated. The melt composition at the beginning of ijolite or nepheline syenite crystallization is reflected in the element concentrations of the cores of clinopyroxene crystals and the composition shortly before complete solidification in those of the rims. Published D^{Cpx} for some elements (Sc, Cr, Co, Sr, Zr, Sm, Eu, Tb, Hf, Ta) vary by an order of magnitude, due either to high analytical uncertainties caused by very low concentrations, or to high sensitivity to comparatively small differences in melt composition and redox conditions. If the magma composition has only a minor influence on the element partitioning between clinopyroxene and melt, the D^{Cpx} are limited to a smaller range. To account for the uncertainties, a minimum and maximum concentration in the melt was calculated for each element (Fig. 14; Table 6).

A comparison of the primitive mantle-normalized trace element compositions between the calculated concentrations of the ijolitic and nepheline syenitic melts with the whole-rock analyses of the primitive host rocks reveals significant enrichments and depletions despite partly high ranges of variation. The observed differences and similarities in the mineral chemistry and in the occurrence of accessory phases are generally well reflected by the calculated element concentrations in the respective melts. Compared to the host rock, the predicted ijolite melt from Urach is markedly enriched in Sr, Hf and Zr, but strongly depleted in Th, U, Ta, LREE, and MREE (Fig. 14). This depletion and Sr enrichment increase with further melt evolution, as shown by the calculated composition of the residual melt in equilibrium with clinopyroxene

Table 5
EPMA analyses of wadeite from Sternberg volcano (Urach). Mineral formulas were calculated based on 9 oxygen and 6 cations with correction for Fe^{3+}.

Analysis	U001–40	U001–41	U001–42	U001–49	U001–50
wt%					
SiO_2	46.20	47.85	48.45	46.82	46.38
TiO_2	1.13	1.67	3.67	3.07	1.27
ZrO_2	26.31	26.64	23.97	23.62	27.06
Al_2O_3	–	–	0.03	–	–
V_2O_3	–	–	0.04	0.01	–
Fe_2O_3	0.24	–	–	0.54	0.15
FeO	–	0.26	0.38	–	–
MnO	0.01	0.03	0.02	–	–
CaO	0.01	0.03	0.03	–	0.01
BaO	0.31	0.31	0.24	0.25	0.24
Na_2O	0.08	–	–	–	–
K_2O	24.02	23.33	24.10	23.97	23.96
Total	**98.30**	**100.12**	**100.93**	**98.28**	**99.07**
apfu					
Si^{4+}	3.067	3.088	3.076	3.069	3.055
Ti^{4+}	0.056	0.081	0.175	0.151	0.063
Zr^{4+}	0.852	0.838	0.742	0.755	0.869
Al^{3+}	–	–	0.002	–	–
V^{3+}	–	–	0.002	0.001	–
Fe^{3+}	0.012	–	–	0.027	0.007
Fe^{2+}	–	0.014	0.020	–	–
Mn^{2+}	0.001	0.002	0.001	–	–
Ca^{2+}	0.001	0.002	0.002	–	0.001
Ba^{2+}	0.008	0.008	0.006	0.006	0.006
Na^{+}	0.011	–	–	–	–
K^{+}	2.034	1.920	1.952	2.004	2.013
Total	**6.041**	**5.953**	**5.980**	**6.013**	**6.015**

– – below detection limit; apfu – atoms per formula unit.

rims. Late Ba enrichment, clearly evidenced by the late-magmatic mineral phase lileyite, cannot be unambiguously reproduced by the calculated melt compositions, probably because published D_{Ba}^{Cpx} are overestimated. The calculated ijolite melt composition for the Hegau case reflects an enrichment of Th, Ta, Nb, Sr, Zr, and Y. When using the minimum D^{Cpx}, the enrichment of all REE and Hf relative to the host rock is also reproduced (Fig. 14b). Predicted Th, Ta, Nb, LREE, and MREE concentrations are significantly higher than for the Urach melt, while Zr and Hf enrichment is lower. Higher Zr/Hf and La/Lu but significantly lower Nb/Ta ratios compared to the Urach ijolite are evident in the incompatible element patterns as well. Modelled compositions of the Kraichgau nepheline syenite melt largely follow that of the Hegau ijolite. Again, minimum D^{Cpx} reproduce the enrichment of most incompatible elements (Th, Ta, Nb, REE, Sr, Hf, Zr) relative to the host rock better. The REE are slightly more and Nb and Ta slightly less enriched compared to the Hegau melt.

The shape of the calculated element patterns of Hegau ijolite and Kraichgau nepheline syenite is similar to that of the nosean phonolites (bimodal Hegau region) and the haüyne phonolites (Odenwald and Kraichgau region) for many incompatible elements (Nb, REE, Hf, Zr; for the Kraichgau case also Th and Ta; Fig. 14b). However, the enrichment of some trace elements in the residual melts exceeds that of the phonolites. An interpretation of the ijolitic or nepheline syenitic melts as missing links in an evolutionary trend towards phonolitic rocks is nevertheless plausible. Positive Pb anomalies and lower enrichment levels for some trace elements are probably due to interaction with crustal lithologies, dilution effects, and late pyrochlore, titanite, and apatite fractionation in upper crustal magma chambers, as suggested by fragments of (nepheline) syenite cumulates in the Hegau phonolites (Binder et al., 2024b). In contrast, such processes were not involved during formation of the coarse-grained ijolitic and nepheline-syenitic domains, so that incompatible elements remained in high concentrations in the small-volume residual melts until complete solidification. Calculated compositions of the ijolitic melts from Urach resemble compositions of agpaitic rocks derived from strongly SiO_2-undersaturated melts elsewhere (e.g., Kola Peninsula, Russia; Pilanesberg, RSA; Poços de Caldas, Brazil; Tamazeght, Morocco), especially regarding high Zr, Hf, and Sr contents, high Nb/Ta ratios and, in contrast, low LREE, MREE, and Th concentrations (Andersen et al., 2017; Filina et al., 2022; Guarino et al., 2021; Marks and Markl, 2017; Wu et al., 2010).

6. Conclusions

Three volcanic edifices in the southern Central European Volcanic Province exhibit coarse-grained domains in the form of mm- to cm-thin veinlets or pockets within the fine-grained to porphyritic primitive host rocks. The following model is proposed for their petrogenesis.

(1) Both ijolites (Hohenstoffeln/Hegau, Sternberg/Urach) and the nepheline syenite (Steinsberg/Kraichgau) are interpreted as differentiates that evolved by separation from the magmas of their respective host rocks – a melilite-bearing olivine-nephelinite, an olivine melilitite, and a phlogopite-nepheline basanite – at crustal levels. This is well documented by the microstructures and the continuous evolution of the mineral assemblage and the chemical composition of the crystallizing phases. The differences and similarities among the three occurrences are partly caused by the initial melt compositions. The proposed differentiation processes occurred without effective gravitational crystal separation compared to fractionation in large magma chambers. This hindered further evolution towards leucocratic, phonolitic compositions. The coarse-grained domains represent the only visible differentiation stage within the three volcanic edifices and separated when the magma compositions were already quite evolved, so that the differentiates do not exhibit a more primitive composition.
(2) The different onset of separation of the ijolitic or nepheline syenitic melts is a key factor regarding trace element evolution and accessory minerals. If the crystallization of clinopyroxene is already advanced and the formation of perovskite in the host rock of the ijolites has already begun (as in the Urach case), then strong fractionation effects cause high Nb/Ta, Zr/Nb, but low LREE/HREE and Zr/Hf ratios in the minerals of the ijolitic product. High F contents contribute to the stabilization of LILE, Zr, and Hf in the residual melt and finally lead to a late-stage agpaitic assemblage of lileyite, wadeite, and Sr-rich fluorapatite. Earlier melt separation before significant perovskite crystallization (as in the Hegau case), however, resulted in a rather uniform enrichment of LILE, HFSE, and REE, concentrated in clinopyroxene and skeletal perovskite and magnetite. The nepheline syenite (Kraichgau) underwent a similar evolution but its mineral assemblage differs from the ijolites due to higher $aSiO_2$ and aH_2O and lower F and P concentrations in the parental melt, with incompatible elements particularly enriched in clinopyroxene and titanite.

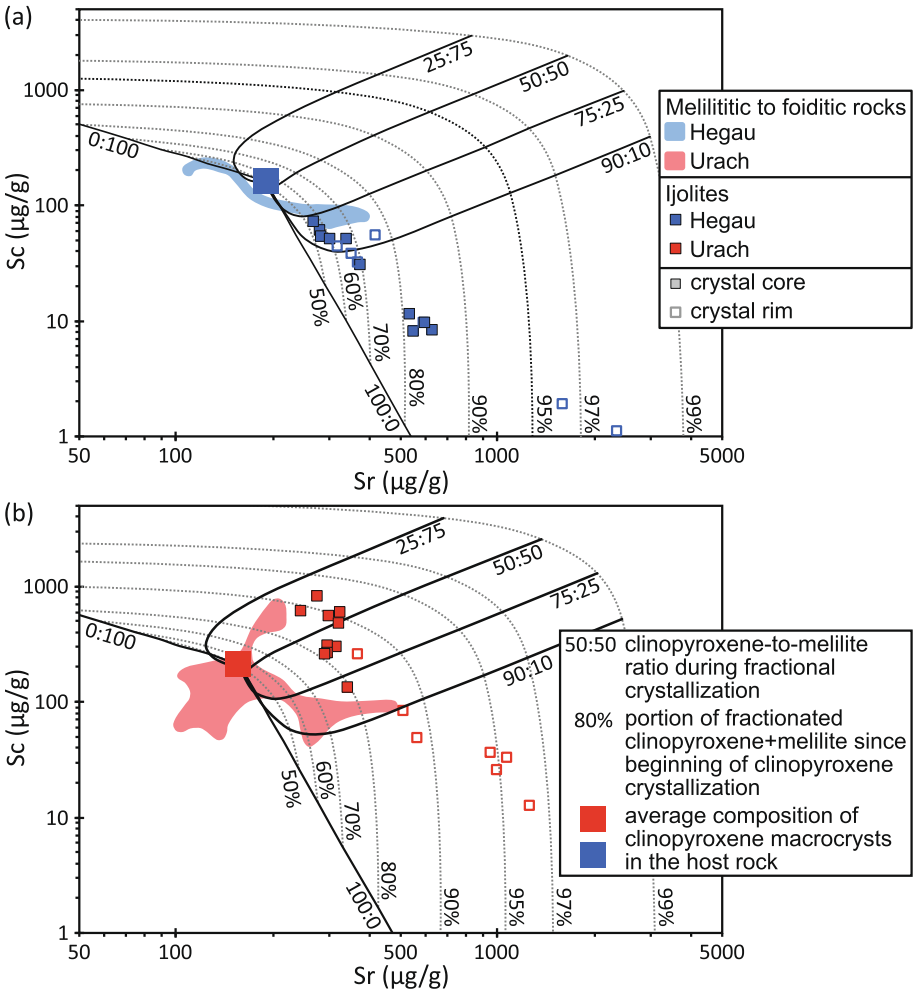

Fig. 13. Sr vs. Sc composition of clinopyroxene in the investigated igneous (a) Hegau and (b) Urach rocks. The differentiation trajectories show the expected evolution of clinopyroxene composition at different ratios of crystallizing clinopyroxene and melilite in the magma assuming Rayleigh fractional crystallization. D^{Cpx} and D^{Mll} are from Minissale et al. (2019). Solid squares represent crystal cores and empty squares crystal rims.

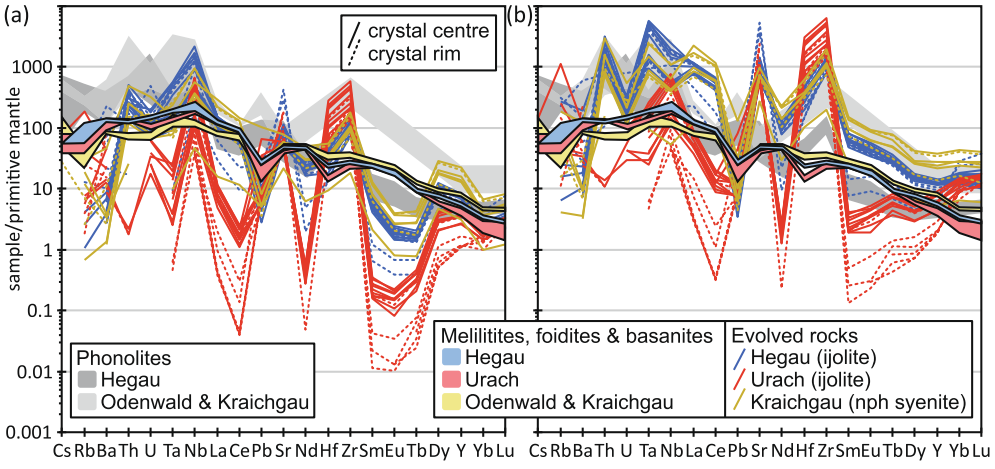

Fig. 14. Comparison of calculated melt compositions for the ijolitic and nepheline syenitic residual melts in equilibrium with clinopyroxene with whole-rock compositions of the three primitive host rocks (Alibert et al., 1983; Binder et al., 2024a; Hegner et al., 1995; Keller et al., 1990; Krause and Weiskirchner, 1981; Walter, 1994). Primitive mantle-normalized incompatible element patterns calculated from clinopyroxene compositions and (a) maximum and (b) minimum D^{Cpx} for evolved alkaline, SiO_2-undersaturated melts (Larsen, 1979; Villemant, 1988; Wörner et al., 1983; normalization values from Palme and O'Neill, 2014). Each pattern is based on one clinopyroxene analysis. For comparison, the compositions of the Hegau and Katzenbuckel phonolites are also shown (Binder et al., 2024b; Keller et al., 1990; Staesche, 1995; Stähle and Koch, 2003).

Table 6
Maximum and minimum partition coefficients for clinopyroxene in evolved alkaline, SiO_2-undersaturated rocks ($D^{Cpx/melt}$) and calculated ijolitic and nepheline syenitic melt compositions in equilibrium with clinopyroxene.

Ele-ment	$D^{Cpx/melt}$		Hegau ijolite (Hohenstoffeln), concentration in ppm				Urach ijolite (Sternberg), concentration in ppm				Kraichgau nepheline syenite (Steinsberg), concentration in ppm			
	max	min	min	max	av. core	av. rim	min	max	av. core	av. rim	min	max	av. core	av. rim
Na	0.10	0.07	25,960	116,283	39,462	54,741	30,588	149,880	45,535	81,924	42,978	115,042	85,200	91,323
Sc	334	6.41	0.00	11	2.9	2.1	0.08	132	34.9	6.5	0.08	17	6.9	8.0
Cr	775	2.88	0.00	28	7.3	2.6		0.68	0.40		0.00	9.7	1.9	9.7
Fe	6.76	6.03	6692	19,344	8448	10,607	6120	13,114	7981	9693	7178	9565	8402	9294
Co	47	1.15	0.54	60	13	17	0.50	38	11	16	0.50	29	23	23
Ni	350	350	0.11	0.26	0.19	0.17	0.09	0.13	0.11	0.10	0.05	0.17	0.09	0.08
Rb	0.04	0.01	0.65	187	28	73	1.1	670	104	21	0.41	113	57	18
Sr	0.25	0.02	1061	117,562	11,132	23,051	976	53,355	8068	20,029	472	21,451	15,139	15,467
Y	1.12	0.66	14	58	41	34	4.5	37	22	9.0	13	155	95	100
Zr	0.55	0.05	755	18,320	7375	6914	909	66,469	20,394	11,278	188	20,033	11,140	12,771
Nb	0.03	0.03	114	1510	624	577	22	461	220	61	28	663	312	437
Cs	0.05	0.03					0.52	2.5			0.50	0.93		
Ba	0.02	0.01	19	4159	151	588	49	1568	242	351	8	835	203	125
La	0.46	0.06	20	802	379	306	0.26	61	24	6.0	11	1533	805	771
Ce	0.96	0.12	16	1158	534	413	0.07	36	14.2	2.9	20	2009	1216	1254
Pr	1.01	0.64	1.6	31	20	15	0.01	0.70	0.41	0.08	3.3	53	34	36
Nd	2.27	0.49	2.7	179	86	63	0.07	3.5	1.6	0.90	8.5	308	203	214
Sm	6.18	0.52	0.29	35	15	11	0.00	1.8	0.64	0.18	0.92	65	44	47
Eu	13.8	0.60	0.07	9.4	3.8	2.9	0.00	0.87	0.33	0.08	0.13	15	11	11
Gd	1.24	0.78	1.9	19	12	9.4	0.08	2.5	1.5	0.40	4.0	37	24	25
Tb	8.63	0.48	0.04	4.0	1.7	1.3	0.00	0.88	0.35	0.10	0.08	8.3	5.4	5.7
Dy	1.09	0.76	2.3	13	10	7.2	0.37	4.4	2.8	0.92	3.4	30	19	20
Ho	1.13	0.71	0.5	2.3	1.6	1.3	0.11	1.1	0.65	0.24	0.57	5.7	3.6	3.8
Er	0.92	0.62	2.7	6.3	4.6	4.1	0.54	3.9	2.5	1.1	1.5	17	10	11
Tm	0.79	0.41	0.42	1.4	0.84	0.79	0.17	0.90	0.54	0.34	0.20	3.3	2.0	2.2
Yb	2.63	0.40	0.72	14	4.1	4.6	0.48	7.1	3.4	2.6	0.47	21	12	14
Lu	2.06	0.41	0.15	2.7	0.61	0.77	0.15	1.3	0.63	0.65	0.09	2.9	1.7	1.7
Hf	1.54	0.14	4.1	147	58	49	11	921	285	133	2.8	186	109	130
Ta	0.30	0.03	0.40	244	75	58	0.02	11	2.8	0.76	0.42	113	48	71
Pb	0.13	0.10	0.51	5.6	1.5	2.2	1.1	15	3.4	2.3	0.66	24	6.8	2.3
Th	0.04	0.01	1.4	268	87	65	0.15	1.2	0.60	0.54	2.2	256	108	106
U	0.03	0.02	1.4	18	3.4	5.5	0.41	2.4	1.2	0.55	1.6	12	5.7	5.9

max – maximum; min – minimum; av. core – concentrations calculated based on the average compositions in clinopyroxene cores and the median of $D^{Cpx/melt}$; av. rim – concentrations calculated based on the average compositions in clinopyroxene rims and the median of $D^{Cpx/melt}$.

(3) The coarse-grained microstructures indicate that differentiation processes occur on a small-volume scale even in quickly ascending and cooling mantle-derived magmas of extremely primitive, alkaline, SiO_2-undersaturated composition. With certain restrictions, the differentiates can be interpreted as a missing link in an evolutionary trend towards nosean phonolites (bimodal Hegau region), phonolitic haüynites, haüyne nephelinites, and haüyne phonolites (Odenwald and Kraichgau).

Supplementary data to this article can be found online at https://doi.org/10.1016/j.lithos.2025.108185.

CRediT authorship contribution statement

Thomas Binder: Writing – review & editing, Writing – original draft, Visualization, Validation, Investigation, Formal analysis, Conceptualization. **Michael A.W. Marks:** Writing – review & editing, Project administration, Conceptualization. **Tobias Fusswinkel:** Writing – review & editing, Writing – original draft, Validation, Resources, Formal analysis. **Benjamin F. Walter:** Writing – review & editing, Validation. **Gregor Markl:** Writing – review & editing, Supervision, Resources.

Funding

This research did not receive any specific grant from funding agencies in the public, commercial, or not-for-profit sectors.

Declaration of competing interest

The authors declare that they have no known competing financial interests or personal relationships that could have appeared to influence the work reported in this paper.

Acknowledgements

We thank the Landesamt für Geologie, Rohstoffe und Bergbau (Freiburg im Breisgau) and Udo Neumann (University of Tübingen) for providing samples used in this study, and Simone Schafflick (University of Tübingen) for sample preparation. Constructive comments by Silvio Mollo, and one anonymous reviewer greatly improved the manuscript and are gratefully acknowledged. We further acknowledge handling by the co-editor-in-chief Greg Shellnutt.

Data availability

The data underlying this article are available at *Mendeley Data* repository (*DOI:10.17632/8d2bhg3hpt.1*). EPMA data was supplemented by literature data from Binder et al. (2024a, 2024b), Mann et al. (2006), and Stähle and Koch (2003).

References

Abratis, M., Viereck, L., Pfänder, J.A., Hentschel, R., 2015. Geochemical composition, petrography and $^{40}Ar/^{39}Ar$ age of the Heldburg phonolite: implications on magma mixing and mingling. Int. J. Earth Sci. (Geologische Rundschau) 104, 2033–2055. https://doi.org/10.1007/s00531-015-1207-x.

Adam, J., Green, T., 2006. Trace element partitioning between mica- and amphibole-bearing garnet lherzolite and hydrous basanitic melt: 1. Experimental results and the

investigation of controls on partitioning behaviour. Contrib. Mineral. Petrol. 152, 1–17. https://doi.org/10.1007/s00410-006-0085-4.
Alibert, C., Michard, A., Albarède, F., 1983. The transition from alkali basalts to kimberlites: isotope and trace element evidence from melilitites. Contrib. Mineral. Petrol. 82, 176–186. https://doi.org/10.1007/BF01166612.
Ambrosio, M.R., Azzone, R.G., 2018. The influence of crystal and melt compositions on the REE+Y partitioning between clinopyroxene and basanitic/tephritic melts of cretaceous alkaline magmatism on the Southeastern part of the South American Platform, Southeast Brazil. Can. Mineral. 56, 303–329. https://doi.org/10.3749/canmin.1700024.
Andersen, T., Erambert, M., Larsen, A.O., Selbekk, R.S., 2010. Petrology of nepheline syenite pegmatites in the Oslo Rift, Norway: zirconium silicate mineral assemblages as indicators of alkalinity and volatile fugacity in mildly agpaitic magma. J. Petrol. 51, 2303–2325. https://doi.org/10.1093/petrology/egq058.
Andersen, T., Elburg, M., Erambert, M., 2017. The miaskitic-to-agpaitic transition in peralkaline nepheline syenite (white foyaite) from the Pilanesberg Complex, South Africa. Chem. Geol. 455, 166–181. https://doi.org/10.1016/j.chemgeo.2016.08.020.
Beckett, J.R., Spivack, A.J., Hutcheon, I.D., Wasserburg, G.J., Stolper, E.M., 1990. Crystal chemical effects on the partitioning of trace elements between mineral and melt: an experimental study of melilite with applications to refractory inclusions from carbonaceous chondrites. Geochim. Cosmochim. Acta 54, 1755–1774. https://doi.org/10.1016/0016-7037(90)90406-B.
Bédard, J.H., Troll, V.R., Deegann, F.M., Tegner, C., Saumur, B.M., Evenchick, C.A., Grasby, S.E., Dewing, K., 2021. High Arctic Large Igneous Province alkaline rocks in Canada: evidence for multiple mantle components. J. Petrol. 62, egab042. https://doi.org/10.1093/petrology/egab042.
Beeskow, M., Wagner, T., Fusswinkel, T., 2022. PySILLS, a newly developed Python-based open source tool for a modern data reduction of LA-ICP-MS experiments. GeoMinKöln 2022. https://doi.org/10.48380/02f5-4x76.
Berger, J., Ennih, N., Mercier, J.-C.C., Liégeois, J.-P., Demaiffe, D., 2009. The role of fractional crystallization and late-stage peralkaline melt segregation in the mineralogical evolution of Cenozoic nephelinites/phonolites from Saghro (SE Morocco). Mineral. Mag. 73, 59–82. https://doi.org/10.1180/minmag.2009.073.1.59.
Binder, T., Marks, M.A.W., Gerdes, A., Walter, B.F., Grimmer, J.C., Beranoaguirre, A., Wenzel, T., Markl, G., 2023. Two distinct age groups of melilitites, foidites and basanites from the southern central European Volcanic Province reflect lithospheric heterogeneity. IInt. J. Earth Sci. (Geologische Rundschau) 112, 881–905. https://doi.org/10.1007/s00531-022-02278-y.
Binder, T., Marks, M.A.W., Walter, B.F., Wenzel, T., Markl, G., 2024a. Two distinct metasomatized mantle sources produced two groups of alkaline SiO_2-undersaturated rocks in the southern central European Volcanic Province. J. Petrol. 65, egae070. https://doi.org/10.1093/petrology/egae070.
Binder, T., Marks, M.A.W., Friedrichsen, B.-E., Walter, B.F., Wenzel, T., Markl, G., 2024b. Bimodal volcanism in the Hegau region (SW Germany): differentiation of primitive melilititic to nephelinitic rocks produces evolved nosean phonolites. Lithos 472-473, 107565. https://doi.org/10.1016/j.lithos.2024.107565.
Blusztajn, J., Hegner, E., 2002. Osmium isotopic systematics of melilitites from the Tertiary central European Volcanic Province in SW Germany. Chem. Geol. 189, 91–103. https://doi.org/10.1016/S0009-2541(02)00143-2.
Braunger, S., Marks, M.A.W., Walter, B.F., Neubauer, R., Reich, R., Wenzel, T., Parsapoor, A., Markl, G., 2018. The petrology of the Kaiserstuhl Volcanic Complex, SW Germany: the importance of metasomatized and oxidized lithospheric mantle for carbonatite generation. J. Petrol. 59, 1731–1762. https://doi.org/10.1093/petrology/egy078.
Büchner, J., Tietz, O., Viereck, L., Suhr, P., Abratis, M., 2015. Volcanology, geochemistry and age of the Lausitz Volcanic Field. IInt. J. Earth Sci. (Geologische Rundschau) 104, 2057–2083. https://doi.org/10.1111/j.1945-5100.2010.01046.x.
Chmyz, L., Azzone, R.G., da Silva Rosa, P.A., Lopes da Silva, J.C., Cetina Tarazona, L.M., Monteiro e Silva, M., 2025. Recycled crystal population proving complex plumbing systems: an archetypal example from Cretaceous alkaline magmatism in SE Brazil. Geol. Soc. Lond. Spec. Publ. 551. https://doi.org/10.1144/SP551-2024-69.
Dawson, J.B., 2008. The Neogene–Recent volcanic rocks. In: Dawson, J.B. (Ed.), The Gregory Rift Valley and Neogene–Recent Volcanoes of Northern Tanzania. Geological Society, London, Memoirs, 33, pp. 39–77. https://doi.org/10.1144/M33.7.
Deer, W.A., Howie, R.A., Zussman, J., 2009. An Introduction to the Rock-Forming Minerals, second ed. Pearson/Prentice Hall, Harlow. https://doi.org/10.1180/DHZ.
Dunworth, E.A., Wilson, M., 1998. Olivine melilitites of the SW German Tertiary Volcanic Province: mineralogy and petrogenesis. J. Petrol. 39, 1805–1836. https://doi.org/10.1093/petroj/39.10.1805.
Egli, D., Mosar, J., Ibele, T., Madritsch, H., 2017. The role of precursory structures on Tertiary deformation in the Black Forest—Hegau region. IInt. J. Earth Sci. (Geologische Rundschau) 106, 2297–2318. https://doi.org/10.1007/s00531-016-1427-8.
Filina, M.I., Kogarko, L.N., Nielsen, T.F.D., 2022. Mineralogical, geochemical, and isotopic data of a new special agpaitic dyke, enriched in high field strength elements (Eastern part of Baltic Shield, Russia). Lithos 428–429, 106828. https://doi.org/10.1016/j.lithos.2022.106828.
Flohr, M.J.K., Ross, M., 1990. Alkaline igneous rocks of Magnet Cove, Arkansas: mineralogy and geochemistry of syenites. Lithos 26, 67–98. https://doi.org/10.1016/0024-4937(90)90041-X.
Giehl, C., Marks, M.A.W., Nowak, M., 2014. An experimental study on the influence of fluorine and chlorine on phase relations in peralkaline phonolitic melts. Contrib. Mineral. Petrol. 167, 977. https://doi.org/10.1007/s00410-014-0977-7.
Gill, R., 2010. Igneous Rocks and Processes – A Practical Guide. Wiley-Blackwell, Chichester. https://doi.org/10.1017/S001675681000066X.
Gornitz, V., 1981. Skeletal crystals. In: Frye, K. (Ed.), Mineralogy. Encyclopedia of Earth Science. Springer, Boston, MA, pp. 469–473. https://doi.org/10.1007/0-387-30720-6_130.
Guarino, V., Lustrino, M., Zanetti, A., Tassinari, C.C.G., Ruberti, E., de Gennaro, R., Melluso, L., 2021. Mineralogy and geochemistry of a giant agpaitic magma reservoir: the Late Cretaceous Poços de Caldas potassic alkaline complex (SE Brazil). Lithos 398–399, 106330. https://doi.org/10.1016/j.lithos.2021.106330.
Guillong, M., Meier, D.L., Allan, M.M., Heinrich, C.A., Yardley, B.W.D., 2008. Appendix 6: SILLS: A MATLAB-based Program for the Reduction of Laser Ablation ICP-MS Data of Homogeneous Materials and Inclusions. Mineralogical Association of Canada, Short Course, 40, pp. 328–333.
Hegner, E., Vennemann, T.W., 1997. Role of fluids in the origin of Tertiary European intraplate volcanism: evidence from O, H, and Sr isotopes in melilitites. Geology 25, 1035–1038. https://doi.org/10.1130/0091-7613(1997)025<1035:ROFITO>2.3.CO;2.
Hegner, E., Walter, H.J., Satir, M., 1995. Pb-Sr-Nd isotopic compositions and trace element geochemistry of megacrysts and melilitites from the Tertiary Urach volcanic field: source composition of small volume melts under SW Germany. Contrib. Mineral. Petrol. 122, 322–335. https://doi.org/10.1007/s004100050131.
Horn, P., Lippolt, H.J., Todt, W., 1972. Kalium-Argon-Altersbestimmungen an tertiären Vulkaniten des Oberrheingrabens. I. Gesamtgesteinsalter. Eclogae Geol. Helv. 65, 131–156.
Jochum, K.P., Stoll, B., Willbold, M., 2007. Validation of LA-ICP-MS trace element analysis of geological glasses using a new solid-state 193 nm Nd:YAG laser and matrix-matched calibration. J. Anal. At. Spectrom. 22, 112–121. https://doi.org/10.1039/B609547J.
Jochum, K.P., Weis, U., Stoll, B., Kuzmin, D., Yang, Q., Raczek, I., Jacob, D.E., Stracke, A., Birbaum, K., Frick, D.A., Günther, D., Enzweiler, J., 2011. Determination of reference values for NIST SRM 610–617 glasses following ISO guidelines. Geostand. Geoanal. Res. 35, 397–429. https://doi.org/10.1111/j.1751-908X.2011.00120.x.
Kato, T., Ringwood, A.E., Irifune, T., 1988. Experimental determination of element partitioning between silicate perovskites, garnets and liquids: constraints on early differentiation of the mantle. Earth Planet. Sci. Lett. 89, 123–145. https://doi.org/10.1016/0012-821X(88)90038-6.
Keller, J., Brey, G., Lorenz, V., Sachs, P., 1990. Volcanism and Petrology of the Upper Rhinegraben (Urach-Hegau-Kaiserstuhl). In: Urach, Hegau, Kaiserstuhl: Excursion 2A, August 27 to September 2, 1990, pp. 1–60.
Keller, J., Zaitsev, A.N., Wiedenmann, D., 2006. Primary magmas at Oldoinyo Lengai: the role of olivine melilitites. Lithos 91, 150–172. https://doi.org/10.1016/j.lithos.2006.03.014.
Klaudius, J., Keller, J., 2006. Peralkaline silicate lavas at Oldoinyo Lengai, Tanzania. Lithos 91, 173–190. https://doi.org/10.1016/j.lithos.2006.03.017.
Krause, O., Weiskirchner, W., 1981. Die Olivin-Nephelinite des Hegaus. Jahreshefte des Geologischen Landesamtes Baden-Württemberg 23, 87–130.
Kuehner, S.M., Laughlin, J.R., Grossman, L., Johnson, M.L., Burnett, D.S., 1989. Determination of trace element mineral/liquid partition coefficients in melilite and diopside by ion and electron microprobe techniques. Geochim. Cosmochim. Acta 53, 3115–3130. https://doi.org/10.1016/0016-7037(89)90093-8.
Larsen, L.M., 1979. Distribution of REE and other trace elements between phenocrysts and peralkaline undersaturmed magmas, exemplified by rocks from the Gardar igneous province, south Greenland (Contribution to the mineralogy of Ilímaussaq, No. 56). Lithos 12, 303–315. https://doi.org/10.1016/0024-4937(79)90022-7.
Le Maitre, R.W., Streckeisen, A., Zanettin, B., Le Bas, M.J., Bonin, B., Bateman, P., Bellieni, G., Dudek, A., Efremov, S., Keller, J., Lameyre, J., Sabine, P.A., Schmid, R., Sørensen, H., Woolley, A.R., 2002. Igneous Rocks: A Classification and Glossary of Terms. Cambridge University Press. https://doi.org/10.1017/CBO9780511535581.
Lustrino, M., Wilson, M., 2007. The circum-Mediterranean anorogenic Cenozoic igneous province. Earth Sci. Rev. 81, 1–65. https://doi.org/10.1016/j.earscirev.2006.09.002.
Mader, S., Ritter, J.R.R., Reicherter, K., AlpArray Working Group, 2021. Seismicity and seismotectonics of the Albstadt Shear Zone in the northern Alpine foreland. Solid Earth 12, 1389–1409. https://doi.org/10.5194/se-12-1389-2021.
Mana, S., Furman, T., Carr, M.J., Mollel, G.F., Mortlock, R.A., Feigenson, M.D., Turrin, B. D., Swisher III, C.C., 2012. Geochronology and geochemistry of the Essimingor volcano: melting of metasomatized lithospheric mantle beneath the North Tanzanian Divergence zone (East African Rift). Lithos 155, 310–325. https://doi.org/10.1016/j.lithos.2012.09.009.
Mann, U., Marks, M.A., Markl, G., 2006. Influence of oxygen fugacity on mineral compositions in peralkaline melts: the Katzenbuckel volcano, Southwest Germany. Lithos 91, 262–285. https://doi.org/10.1016/j.lithos.2005.09.004.
Marks, M.A.W., Markl, G., 2017. A global review on agpaitic rocks. Earth Sci. Rev. 173, 229–258. https://doi.org/10.1016/j.earscirev.2017.06.002.
Mäussnest, O., 1974. Die Eruptionspunkte des Schwäbischen Vulkans – Teil I. Z. Dtsch. Ges. Geowiss. 125, 23–54.
Mäussnest, O., Schreiner, A., 1982. Karte der Vorkommen von Vulkangesteinen im Hegau. Abhandlungen des Geologischen Landesamtes Baden-Württemberg 10, 1–48.
Mazzeo, F.C., Rocco, I., Tucker, R.D., Morra, V., D'Antonio, M., Melluso, L., 2021. Olivine melilitites, mantle xenoliths, and xenocrysts of the Takarindiona district: petrogenesis, magmatic evolution, and the sub-continental lithospheric mantle of east-Central Madagascar. J. Afr. Earth Sci. 174, 104059. https://doi.org/10.1016/j.jafrearsci.2020.104059.
Melluso, L., Le Roex, A.P., Morra, V., 2011. Petrogenesis and Nd-, Pb-, Sr-isotope geochemistry of the Cenozoic olivine melilitites and olivine nephelinites

("*ankaratrites*") in Madagascar. Lithos 127, 505–521. https://doi.org/10.1016/j.lithos.2011.08.003.
Minissale, S., Zanetti, A., Tedesco, D., Morra, V., Melluso, L., 2019. The petrology and geochemistry of Nyiragongo lavas of 2002, 2016, 1977 and 2017 AD, and the trace element partitioning between melilitite glass and melilite, nepheline, leucite, clinopyroxene, apatite, olivine and Fe-Ti oxides: a unique scenario. Lithos 332-333, 296–311. https://doi.org/10.1016/j.lithos.2019.02.023.
Mourey, A.J., France, L., Ildefonse, B., Gurenko, A., Laporte, D., 2023. Genesis of carbonatite at Oldoinyo Lengai (Tanzania) from Olivine Nephelinite: protracted melt evolution and reactive porous flow in deep crustal mushes. J. Petrol. 64, egad084. https://doi.org/10.1093/petrology/egad084.
Nagasawa, H., Schreiber, H.D., Morris, R.V., 1980. Experimental mineral/liquid partition coefficients of the rare earth elements (REE), Sc and Sr for perovskite, spinel and melilite. Earth Planet. Sci. Lett. 46, 431–437. https://doi.org/10.1016/0012-821X(80)90056-4.
Neave, D.A., Putirka, K.D., 2017. A new clinopyroxene-liquid barometer, and implications for magma storage pressures under Icelandic rift zones. Am. Mineral. 102, 777–794. https://doi.org/10.2138/am-2017-5968.
Nielsen, R.L., 1992. BIGD.FOR: a FORTRAN program to calculate trace-element partition coefficients for natural mafic and intermediate composition magmas. Comput. Geosci. 18, 773–788. https://doi.org/10.1016/0098-3004(92)90024-L.
Palme, H., O'Neill, H., 2014. Cosmochemical estimates of mantle composition. In: Holland, H.D., Turekian, K.K. (Eds.), The Mantle and Core. Elsevier, pp. 1–39.
Platz, T., Foley, S.F., André, L., 2004. Low-pressure fractionation of the Nyiragongo volcanic rocks, Virunga Province, D.R. Congo. J. Volcanol. Geotherm. Res. 136, 269–295. https://doi.org/10.1016/j.jvolgeores.2004.05.020.
Putirka, K.D., 2008. Thermometers and barometers for volcanic systems. Rev. Mineral. Geochem. 69, 61–120. https://doi.org/10.2138/rmg.2008.69.3.
Rupf, I., Nitsch, E., 2008. Das Geologische Landesmodell von Baden-Württemberg: Datengrundlagen, technische Umsetzung und erste geologische Ergebnisse. LGRB-Informationen 21, 1–82.
Schmincke, H.-U., 2007. The quaternary volcanic fields of the East and West Eifel (Germany). In: Ritter, J.R.R., Christensen, U.R. (Eds.), Mantle Plumes. Springer, Berlin, Heidelberg, pp. 241–322. https://doi.org/10.1007/978-3-540-68046-8_8.
Schmitt, A.K., Marks, M.A., Nesbor, H.D., Markl, G., 2007. The onset and origin of differentiated Rhine Graben volcanism based on U-Pb ages and oxygen isotopic composition of zircon. Eur. J. Mineral. 19, 849–857. https://doi.org/10.1127/0935-1221/2007/0019-1776.
Schmitt, F., Marks, M.A.W., Siegel, M., Henzler, M., Zaitsev, A.N., Markl, G., 2024. Nephelinites from Burko volcano (Tanzania) record the phase relations among perovskite, magnetite, titanite and andradite in evolved alkaline and silica-undersaturated systems. Geochemistry 84, 126211. https://doi.org/10.1016/j.chemer.2024.126211.
Sliwinski, J.T., Bachmann, O., Ellis, B.S., Dávila-Harris, P., Nelson, B.K., Dufek, J., 2015. Eruption of shallow crystal cumulates during explosive phonolitic eruptions on Tenerife, Canary Islands. J. Petrol. 56, 2173–2194. https://doi.org/10.1093/petrology/egv068.
Staesche, A., 1995. Der genetische Zusammenhang zwischen Melilithiten und Phonolithen des Hegaus, SW-Deutschland. Diploma thesis. Tübingen, 66 pp.
Stähle, V., Koch, M., 2003. Primary and secondary pseudobrookite minerals in volcanic rocks from the Katzenbuckel Alkaline Complex, southwestern Germany. Schweizerische Mineralogische und Petrographische Mitteilungen (Swiss Bulletin of Mineralogy and Petrology) 83, 145–158.
Ulrych, J., Pivec, E., Lang, M., Lloyd, F.E., 2000. Ijolitic segregations in melilite nephelinite of Podhorni vrch volcano, Western Bohemia. Neues Jahrbuch für Mineralogie – Abhandlungen (Journal of Mineralogy and Geochemistry) 175, 317–348. https://doi.org/10.1127/njma/175/2000/317.
Ulrych, J., Lloyd, F.E., Balogh, K., Hegner, E., Langrová, A., Lang, M., Novák, J.K., Řanda, Z., 2005. Petrogenesis of alkali pyroxenite and ijolite xenoliths from the Tertiary Loucna–Oberwiesenthal Volcanic Centre, Bohemian Massif in the light of new mineralogical, geochemical, and isotopic data. Neues Jahrbuch für Mineralogie – Abhandlungen (Journal of Mineralogy and Geochemistry) 182, 57–79. https://doi.org/10.1127/0077-7757/2005/0029.
Vaněčková, M., Holub, F.V., Souček, J., Bowes, D.R., 1993. Geochemistry and petrogenesis of the tertiary alkaline volcanic suite of the Labe tectonovolcanic zone, Czech Republic. Mineral. Petrol. 48, 17–34. https://doi.org/10.1007/BF01164906.
Villemant, B., 1988. Trace element evolution in the Phlegrean Fields (Central Italy): fractional crystallization and selective enrichment. Contrib. Mineral. Petrol. 98, 169–183. https://doi.org/10.1007/BF00402110.
Vuorinen, J.H., Hålenius, U., Whitehouse, M.J., Mansfeld, J., Skelton, A.D.L., 2005. Compositional variations (major and trace elements) of clinopyroxene and Ti-andradite from pyroxenite, ijolite and nepheline syenite, Alnö Island, Sweden. Lithos 81, 55–77. https://doi.org/10.1016/j.lithos.2004.09.021.
Walter, H.-J., 1994. Spurenelement- und Isotopengeochemie von Megakristallen und Melilithiten des Uracher Vulkangebietes: Signifikanz für die Genese des tertiären zentraleuropäischen Vulkanismus. Diploma thesis.. Eberhard Karls Universität Tübingen, Tübingen.
Wang, X., Hou, T., Wang, M., Zhang, C., Zhang, Z., Pan, R., Marxer, F., Zhang, H., 2021. A new clinopyroxene thermobarometer for mafic to intermediate magmatic systems. Eur. J. Mineral. 33, 621–637. https://doi.org/10.5194/ejm-33-621-2021.
Wörner, G., Beusen, J.-M., Duchateau, N., Gijbels, R., Schmincke, H.-U., 1983. Trace element abundances and mineral/melt distribution coefficients in phonolites from the Laacher See Volcano (Germany). Contrib. Mineral. Petrol. 84, 152–173. https://doi.org/10.1007/BF00371282.
Wu, F.-Y., Yang, Y.-H., Marks, M.A.W., Liu, Z.-C., Zhou, Q., Ge, W.-C., Yang, J.-S., Zhao, Z.-F., Mitchell, R.H., Markl, G., 2010. *In situ* U–Pb, Sr, Nd and Hf isotopic analysis of eudialyte by LA-(MC)-ICP-MS. Chem. Geol. 273, 8–34. https://doi.org/10.1016/j.chemgeo.2010.02.007.